Fundamental Studies of Nanofluidics: Nanopores, Nanochannels, and Nanopipets

Daniel G. Haywood, Anumita Saha-Shah, Lane A. Baker,* and Stephen C. Jacobson*

Department of Chemistry, Indiana University, Bloomington, Indiana 47405-7102, United States

CONTENTS

Ion, particle, and fluid transport in nanofluidic devices has received considerable attention over the past two decades due to unique transport properties exhibited at the nanoscale.[1,2] Phenomena such as double layer overlap, high surface-to-volume ratios, surface charge, ion-current rectification, and entropic barriers can influence transport in and around nanofluidic structures because the length scales of these forces and the critical dimensions of the device are similar. Advances in micro- and nanofabrication techniques provide the ability to design a variety of well-defined nanofluidic geometries to study these phenomena and their effects on ion and fluid transport. Integration of micro- and nanofluidic structures into lab-on-a-chip devices permits increased functionality that is useful for a range of analytical applications.[3,4] This Review focuses on recent advances in nanofabrication techniques as well as studies of fundamental transport in nanofluidic devices. Nanopores, nanochannels, and nanopipets are three common nanofluidic structures that have been influential in studying nanofluidic transport. Because of space limitations, we have limited the scope of this Review to studies with these three structures, and we focus our attention primarily on work published between January 2011 and August 2014. We do not discuss work with carbon nanotubes,[5] nanomeshes,[6] or nanowires.[7]

Figure 1 shows examples of the three nanofluidic geometries discussed here. Nanopores are typically formed perpendicular to the plane of a substrate and are characterized by a critical limiting dimension, which is measured by scanning electron microscopy (SEM), transmission electron microscopy (TEM), or conductance measurements. Pores are fabricated in a variety of materials, e.g., poly(carbonate), poly(ethylene terephthalate), or silicon nitride, and can have an asymmetric (Figure 1a) or symmetric (Figure 1b) shape, depending on the fabrication technique. Symmetric pores are either cylindrically shaped with a constant critical dimension determined by electron microscopy or hourglass-shaped with a critical dimension at the center of the pore. Although electron microscopy is capable of measuring exterior pore dimensions, the exact inner geometry is often unknown and may contain an asymmetry between two symmetric features, e.g., cigar-shaped pores. Asymmetric nanopores typically have a narrow tip and a wide base with a funnel-shaped geometry along the pore axis. Tip and base dimensions are measured by SEM, but the exact pore geometry is often unknown. Nanochannels often refer to in-plane structures with either symmetric (Figure 1c) or asymmetric (Figure 1d) geometries. Channels may be confined to the nanoscale in depth, width, or both, depending on the fabrication method. Nanochannels are commonly fabricated in glass and polymer substrates and characterized by SEM and atomic force microscopy (AFM). The in-plane nature of these channels allows the integration of well-defined features into more complex geometries, and any two-dimensional (2D) channel architecture can be designed. Nanopipets are specialized nanopores fabricated from pulled glass or fused-silica capillaries (Figure 1e,f). The geometry of a nanopipet is conically shaped with a critical tip diameter of tens to hundreds of nanometers, which can be measured by electron microscopy. Unlike nanopores and nanochannels, nanopipets can be easily coupled with position control, which allows the tip of the nanopipets to be positioned in specific locations or used in scanned probe microscopies.

ADVANCES IN NANOFABRICATION

Increased availability and sophistication of nanofabrication techniques have contributed significantly to the recent growth of nanofluidics.[8] Although colloid and membrane sciences have explored nanofluidic phenomena with nano- and microparticles
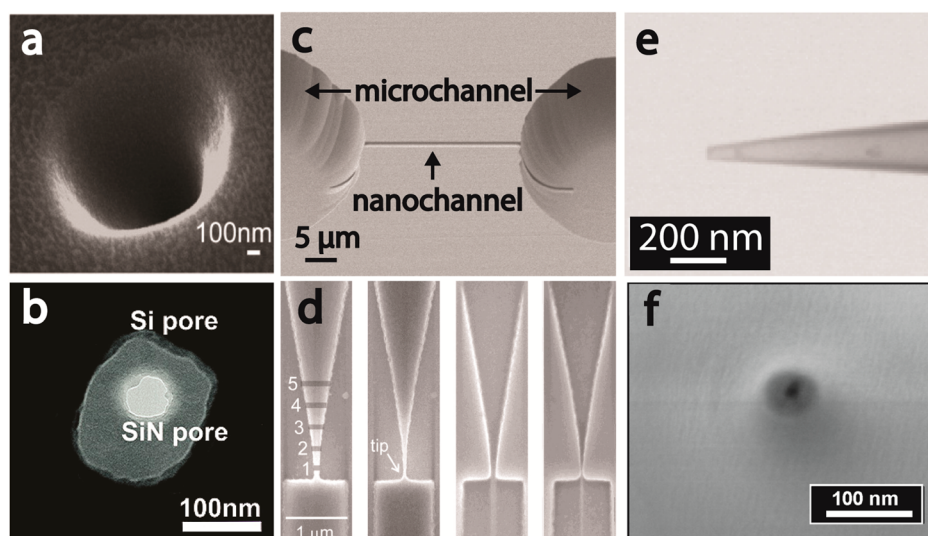
Figure 1. Nanopores, nanochannels, and nanopipets are three common nanofluidic platforms. Nanopores are typically out-of-plane structures and have either an asymmetric or symmetric geometry. Conical nanopores have a wide base as shown in panel a that tapers to a critical nanometer-sized tip. Reprinted from ref 24. Copyright 2012 American Chemical Society. Symmetric nanopores, similar to the SiN pore in panel b, have a circular geometry with a nanometer-scale diameter. Reprinted with permission from ref 186. Copyright 2011 American Chemical Society. Nanochannels are commonly fabricated as in-plane structures. (c) A rectangular nanochannel is milled in a glass substrate between two microchannels by a focused ion beam instrument. (d) Asymmetric nanochannels fabricated by electron-beam lithography, polymer replication, and electron-beam induced etching have a wide base and a narrower, critical tip dimension. Reprinted with permission from ref 34. Copyright 2012 John Wiley & Sons, Inc. Nanopipets have asymmetric geometries that taper toward a critical tip diameter. Quartz capillaries are pulled to fabricate nanopipets with inner diameters below 75 nm, which are used for (e) electrospray ionization of peptides and (f) discrimination of charged surfaces. Panel e is reprinted from ref 248. Copyright 2013 American Chemical Society. Panel f is reprinted from ref 127. Copyright 2011 American Chemical Society.

and in porous media for many decades, fabrication methods to form individual, well-defined nanoscale structures are a major development over the past two decades. A variety of methods including high-energy beam milling, damage-track etching, dry and wet etching, laser writing, laser pulling, and imprint lithography have become established nanofabrication techniques and remain widely used in nanofluidic research as discussed in previous reviews.[1,2,9] Recent developments in nanofabrication seek to improve device-to-device reproducibility, decrease critical dimensions, and ease device production. In this section, we summarize recent advances in existing nanofabrication techniques in addition to new nanofabrication methods developed in the time frame of this Review for the three nanofluidic geometries described above.

Nanopores. Fabrication methods such as high-energy beam milling or selective etching of ion tracks through a polymer membrane are commonly used to fabricate nanopores perpendicular to the substrate surface. Sculpting fabricated pores by low energy ion- or electron-beam irradiation allows both the shape and size of these pores to be tuned to a desired geometry.

Transmission electron microscopes can fabricate sub-10 nm nanopores by irradiating a thin membrane with a focused, high-energy beam of electrons.[10] Ablation of the membrane results in the formation of an individual nanopore. Milling through a metal film deposited onto a silicon nitride membrane is used to create nanogap electrodes adjacent to a pore for enhanced functionality.[11,12] Drilled pores are tuned with electron-beam sculpting which uses a low energy electron beam (e-beam) to controllably close a larger opening to single-nanometer dimensions.[13,14] A focused ion beam (FIB) instrument is also able to mill single nanopores in thin membranes by two primary methods. Typical ion-beam drilling with gallium ions produces individual nanopores with diameters of tens of

nanometers,[15] and narrowing of these pores is possible by atomic layer deposition.[16] FIB milling can also produce pores as small as 6 nm in diameter in cooled substrates (<173 K) due to reduced surface diffusion.[17] Helium ion beam milling drills nanopores directly in unprocessed silicon nitride membranes and generates pores with diameters <4 nm with low electronic noise.[18] Nanopores milled in silicon nitride membranes by a helium ion beam also have reduced background fluorescence compared to pores milled with gallium ions.[19] Similar to e-beam sculpting, ion-beam sculpting employs a low energy ion beam to precisely close an opening to diameters as small as 1–2 nm.[20] Pores sculpted by an e-beam form a hydrocarbon layer, effectively lengthening the pore, whereas pores sculpted by an ion beam incorporate gallium ions and become hourglass shaped with a wider average pore diameter compared to pores drilled directly.[21] Nanopores are also formed by selective ion-track etching in thin membranes and are widely used for current-rectification studies. A drawback to the use of track-etched pores is the unknown inner pore geometry. Conductance measurements and SEM observations more accurately reconstruct and predict the longitudinal geometry of pores in track-etched membranes, which has a direct impact on rectification.[22] The geometries of pores in track-etched membranes can be tuned to a degree, where asymmetric etching of polymer membranes creates funnel-shaped pores and single-sided surfactant-assisted etching produces bullet-like pores.

Alternative methods to fabricate nanopores aim to decrease fabrication time and production cost. Single nanopores are fabricated by nanofractures in commercially available capillaries as an inexpensive nanofabrication method.[23] Metal nanoparticle-assisted plasma etching produces conically shaped nanopores in silicon substrates.[24] Conventional photolithography and wet chemical etching generate arrays of pyramidal

nanopores with an average side length of 60 nm, which are employed as a reusable lithography mask.[25] Nanoapertures are also produced by a low cost, corner lithography technique in which isotropic thinning generates a nitride nanodot which is removed to form a nanoscale opening.[26] Nanoporous materials such as anodized aluminum oxide[27] can be modified by atomic layer deposition to effectively reduce pore diameters[28] and increase performance.[29]

Nanochannels. Nanochannels are ideal geometries for investigating fundamental transport and biological sensing[30] due to the ability to control and characterize all three channel dimensions. Additionally, nanochannels in the plane of the substrate allow optical measurements to be combined with electrical measurements to provide complementary information. One-dimensional (1D) and two-dimensional (2D) nanochannels are fabricated in-plane by a variety of methods. Conventional microfabrication techniques such as photolithography and wet chemical etching are used to fabricate 1D nanoscale-depth microchannels,[31] but techniques such as e-beam lithography and focused ion beam milling are typically needed to fabricate 2D structures that are confined to the nanoscale in both lateral dimensions.

Electron beam lithography (EBL) uses an electron beam to replicate a desired pattern on a surface coated with a thin, electron-sensitive resist. Fabrication of 2D nanochannels is achieved by either selective removal of the exposed positive-tone resist or unexposed negative-tone resist. Removal of exposed positive-tone resist uncovers only the desired sections of the substrate, and the nanochannel design can be directly transferred to the substrate, for example, by reactive ion etching (RIE).[32] Conversely, removal of unexposed negative-tone resist leaves raised nanofluidic features on the substrate. The pattern on the substrate is then used as a master to mold nanofluidic channels in polymer materials.[33] Nanofluidic masters can also be shaped by e-beam induced etching to produce smaller critical dimensions.[34] EBL can also deposit metal films onto a substrate by e-beam deposition[35] to form nanogap electrodes in nanochannel arrays.[36]

Similarly, FIB milling can fabricate 2D nanochannels in any arbitrary pattern. A beam of focused ions, commonly Ga ions, is rastered along a specified pattern, directly milling the feature into the substrate. Channel depth is precisely controlled by varying either the beam current or the dose of ions that impinge the surface. Charging of insulating materials due to the accumulation of ions on the substrate surface is circumvented by deposition of a conductive sacrificial layer, e.g., a metal film, onto the substrate or bathing the surface with electrons during milling.[37] Milling through a sacrificial layer[38,39] minimizes redeposition of material during milling and reduces swelling. Channels less than 5 nm wide are milled with an FIB instrument in quartz through a relatively thick metal film, e.g., 100 nm, which takes advantage of the narrowed width of structures milled deeper into a substrate.[40] FIB milling can also create masters from which polymer nanochannel devices are cast.[41−43]

Similar to nanopore fabrication, alternative methods for nanochannel fabrication are being explored to increase throughput and decrease production costs. EBL and FIB milling provide precise features but are both expensive and time-consuming processes. Nanochannels with high lateral fidelity are fabricated by nanoimprint lithography (NIL).[44,45] Unlike EBL and FIB milling, NIL is a high-throughput technique used to fabricate 1D and 2D nanochannels by mechanically pressing a fabricated master into a curable resist.[46] The master is somewhat expensive and time-consuming to produce but is able to replicate a number of devices. Imprint resist spun onto a substrate is brought into physical contact with a master, and the resist is cured leaving the imprinted nanochannel structures in the resist layer. A hybrid fabrication process that combines hot embossing and inverse UV-lithography forms micro- and nanochannels in SU-8 from a master with high reproducibility.[47] Stacking of exfoliated graphene oxide sheets has successfully created massive arrays of nanochannels.[48] Microcontact printing of an alkane monolayer onto a mica surface is a cost-effective technique to produce 1D nanochannels.[49]

Nanopipets. Nanopipets are fabricated from glass or quartz capillaries by application of heat to soften the capillary followed by physically pulling the capillary to separate the capillary into two sister pipets. Mechanical pullers provide precise control over the fabrication process with heat provided by a metal filament or laser source. Control over pulling parameters allows the pipet geometry to be tuned to a degree with different parameters providing different taper lengths and opening diameters. After being pulled, the pipet tip geometry can be further tuned with microforges or through polishing to alter the tip geometry.[50] More advanced methods such as ion or electron beam radiation[51] and FIB milling[52,53] also shape pipet tips with high precision.

Additional functionality is imparted on nanopipets by deposition of electrode material or functionalization of the glass surface with specific chemical recognition elements. Several strategies have been explored to deposit carbon and metal films to obtain nanoelectrodes that combine high-resolution imaging with chemical analysis through scanning ion conductance microscopy (SICM) or scanning electrochemical microscopy (SECM). Flowing gases such as methane, acetylene, or butane inside the pipet and subsequent pyrolysis of the gas deposits carbonaceous material on the inner wall of a nanopipet.[54,55] Changing the ratio of methane to carrier gas and pyrolysis time influences the amount of carbon deposited inside the nanopipet tip.[56] A 1:1 ratio of methane to argon gas produces nanoelectrodes with carbon layers on the inner wall of the quartz pipet that blocked the pipet channel and contained a cavity at the tip of the pipet. Cavity depth depends on tip diameter and pipet geometry. However, a relatively short chemical vapor deposition (CVD) time of 30 min and a lower methane to argon ratio yield pipets with an open path in the middle. The cavity at the tip is able to sample nanoliter volumes of sample through capillary action. Carbon ring electrodes are fabricated by CVD of parylene C onto a nanopipet, followed by pyrolysis of the parylene C layer at 900 °C under an inert nitrogen atmosphere to form a conformal layer of amorphous carbon. The carbon ring electrode is exposed by FIB milling of the nanopipet tip after deposition of an insulating layer of parylene C.[53] Metal-ring electrodes are formed by thermally evaporating or sputtering a conductive metal layer onto a pipet, depositing an insulating layer around the metal, and exposing the end of the capillary by FIB milling.[57] Metal electrodes can also be formed at the tip of carbon coated nanopipets by electrochemical deposition of platinum at the nanopipet tip.[58] A metal disk shaped electrode can be fabricated at the tip of a nanopipet by electroless deposition of gold nanoparticles at a liquid−liquid interface supported by the nanopipet. The metal precursor is present in an aqueous phase, the reductant is present in an organic phase, and potential developed at the

174

dx.doi.org/10.1021/ac504180h | *Anal. Chem.* 2015, 87, 172−187

interface leads to spontaneous formation of metal nanoparticles which block the tip of the pipet, forming a disk-shaped nanoelectrode.[59]

■ ELECTROKINETIC EFFECTS

Transport at the nanoscale is uniquely affected by physical phenomena such as surface charge, double layer overlap, and ion current rectification, which are typically absent or insignificant in microfluidic devices. Fundamental studies of these forces are essential to design nanofluidic devices effective for analytical applications. Here, we provide a brief overview of electrostatic and electrokinetic effects and focus on how they impact transport through nanofluidic structures.

Electrical Double Layer. Fixed charges on a surface attract oppositely charged ions in solution, creating an electrical double layer (EDL) to maintain electrical neutrality. The potential distribution within the counterion-rich double layer is described by the Poisson–Boltzmann equation and decays away from the surface. Surface charge density and electrolyte concentration affect the thickness of the EDL, which is typically on the order of 1–30 nm.[60] Double layers are thin at high salt concentrations and low surface charge density but increase in thickness with lower salt concentrations and higher surface charge density. In nanofluidic structures, double layers on opposite surfaces can interact and even overlap, which can create permselective openings that repel co-ions. The structure of the double layer dictates nanofluidic transport; consequently, the impact of solution composition and surface modification on EDL structure is of great interest.

A nanochannel sandwiched between a pair of sensing electrodes is used to study the effects of decreasing ion concentration on EDL structure.[61] As predicted by theory, decreased ion concentration causes expansion of the EDL, which can merge with the EDL associated with the opposing electrode. Proton distributions near a glass wall are captured by super-resolution laser-induced fluorescence to gain insight into the EDL structure.[62] In nanocapillaries, impedance spectroscopy probes capacitance and geometric effects which are resolved by varying the electrolyte concentration.[63]

Conductivity. Previous studies have shown that nanochannels exhibit higher conductivity than bulk ionic solutions at low electrolyte concentrations due to a large portion of current carried in the double layer by counterions.[64] As channel dimensions decrease, the contribution of surface charge becomes greater, and a lower threshold conductance is observed.[65,66]

Surface-charge governed ion transport occurs in nanochannels fabricated with layered materials.[48] This effect influences transport not only in a nanofluidic structure but also affects transport away from the structure. Electric current is perturbed at a distance from a nanopore dictated by the Dukhin length in order to meet charge conservation at a pore entrance.[67] Chemical modification can reduce overall surface charge which, in turn, reduces channel conductivity.[66] Simulations predict that long channels modified with polyelectrolyte chains exhibit higher conductance due to the increased number of counterions necessary to balance the charge, but channels modified with neutral polymers have a lower overall conductance.[68]

Electroosmotic Flow. Application of an electric field along a fluidic conduit with surface charge induces movement of mobile ions in the electrical double layer, and viscous forces in solution drag adjacent fluid layers along in the same direction, creating electroosmotic flow (EOF). The profile of EOF in microchannels is plug-like, and velocity increases as ionic strength decreases. However, EOF in a nanochannel is influenced when the double layer extends into the channel at low salt concentrations, giving rise to parabolic flow profiles that mirror the potential distribution and result in a reduced average velocity.[69−71] EOF at low ionic strength is reduced in rectangular nanochannels with half-depths <100 nm when compared to EOF in microchannels.[37] Electroosmotic mobilities in the nanochannels exhibit maxima at $\kappa h \sim 4$, where κ is the Debye−Hückel parameter and h is the channel half-depth, indicating that the degree of double layer overlap depends on both channel dimensions and Debye length.

Physical factors that affect electroosmotic flow have been investigated theoretically. Changes in surface properties that affect EOF are induced by field-effect control, and models predict that the EOF velocity can be tuned by a nanofluidic field-effect transistor.[72] Surface modifications modulate EOF, and simulations of channels with polyelectrolyte coatings predict different flow profiles compared to bare nanochannels.[73] Mismatched EOF at the junction of a microchannel and nanochannel results in a pressure gradient which improves separation efficiency in nanofluidic channels.[74] This pressure gradient can be used for electroosmotically induced pumping and increased flow rates at low voltages.[75]

Electrophoresis. Electrophoresis is the movement of charged particles in an electric field and separates particles based on charge and hydrodynamic volume. The electrophoretic mobility of particles can be reduced in nanochannels due to interactions with the channel surface and electrical double layer.[76] Electrophoresis of rigid spheres is studied numerically, and previous models are extended to include effects of multi-ion species.[77] These studies also suggest that particle mobility depends on the magnitude and direction of EOF. Another model of electrophoretic motion examines the effects of surface potential and double-layer thickness on transport. This model concludes that higher viscosity droplets travel more slowly, and droplets with lower surface potential actually induce faster particle movement due to ions being drawn into the double layer, which decreases polarization effects.[78]

Streaming Potential. Pressure-driven flow through channels or nanopores creates an electric streaming current due to the movement of ions in the bulk and EDL. Accumulation of ions downstream generates an electric streaming potential that depends on surface charge, electrolyte concentration, and channel dimensions.[79] With these factors, streaming potential measurements can be used to calculate the zeta potential of channels.

Double layer overlap leads to a decrease in the streaming potential and must be accounted for by correction factors.[69] Simulations show an increase in the magnitude of streaming potential in ion-selective nanopores, which is attributed to the finite size of ionic species and must be accounted for in numerical predictions.[80,81] Sidewalls lead to a decrease in streaming potential in low aspect-ratio channels due to the reduction in pressure-driven velocity.[82] Analytical solutions to quantify streaming potential and electroviscous effects that account for EDL thickness predict three regimes of EDL influence on the streaming potential that depend on conduction current.[83] In cases of strong double layer overlap ($\kappa a \sim 1$, where a is the capillary radius), the effective viscosity is
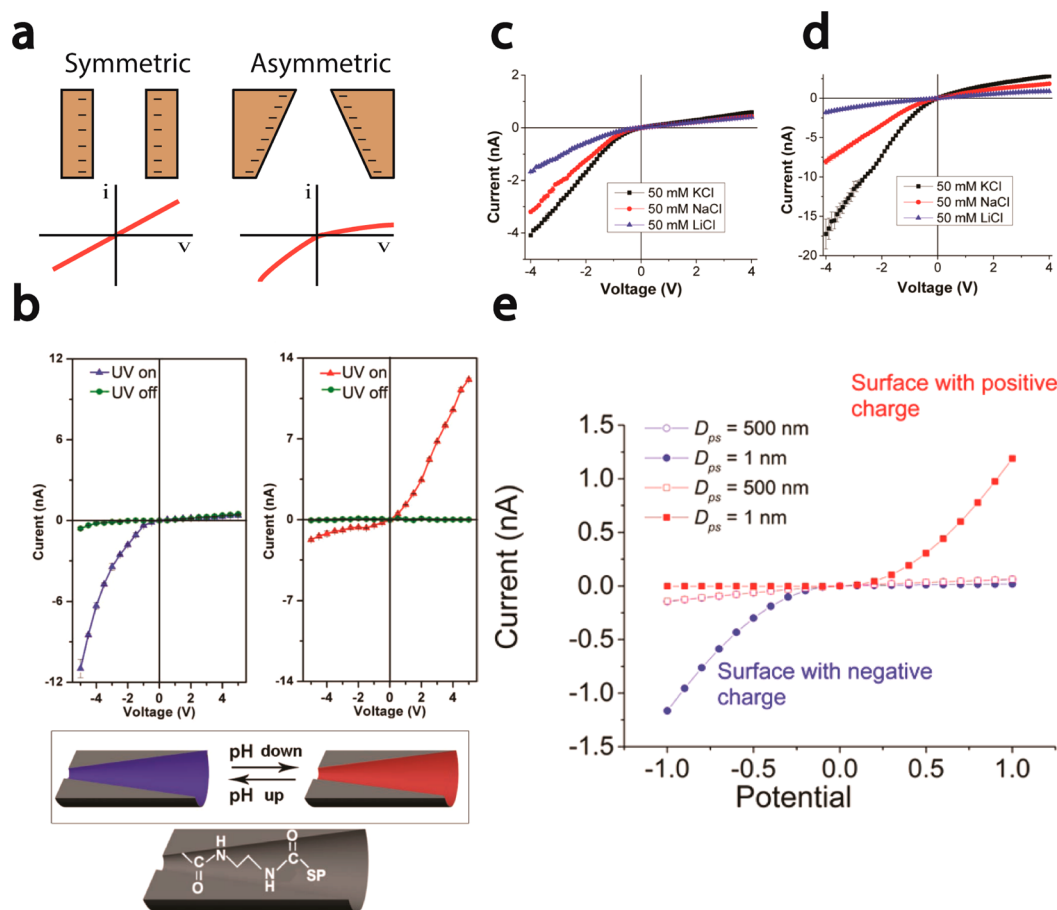
Figure 2. Ion-current rectification is preferential current transport in nanofluidic structures that have an asymmetry in geometry (panel a), surface charge, or blockage of an opening. (b) Conical nanopores modified with a spiropyran molecule rectify ion current when illuminated with UV light, and ion current rectification changes direction when pH is changed. Reprinted with permission from ref 100. Copyright 2012 John Wiley & Sons, Inc. (c) Simulations and (d) experiments show that the magnitude of ion current rectification in nanopores with single-nanometer diameters depends on cation size. Reprinted from ref 113. Copyright 2014 American Chemical Society. (e) Ion-current rectification at the interface between a nanopipet and a charged surface occurs in opposite directions for oppositely charged surfaces. Reprinted from ref 128. Copyright 2013 American Chemical Society.

governed by the EOF velocity, and competing flows in opposite directions reduce overall net flow.

Ion-Current Rectification. Ion-current rectification (ICR) is a result of uneven transference of cations and anions across a nanostructure, and ion current is greater in one direction than in the other (Figure 2a).[84] ICR is observed in nanofluidic devices that contain either an asymmetric geometry, asymmetric surface charge, physical blockage near the nanostructure, or a combination of these features. ICR was first observed in quartz nanopipet electrodes[85] and later studied extensively with conically shaped nanopores in polymer membranes.[86] The degree to which a device rectifies current is quantified by the rectification ratio, which is the absolute value of the ratio of ion current measured at two applied potentials of equal magnitude but opposite polarity. ICR is analogous to solid-state electronic diodes, and fabrication of nanofluidic devices with diode-like behavior is of particular interest.

The extent and direction of rectification depends on surface charge density,[87] scan rate,[88] and polarity of the applied potential and can be controlled by changes in electrolyte concentration,[89] solution pH,[90] surface modification,[91] and field-effect modulation.[92] ICR is influenced by surface modifications that affect the surface charge of the device and alter the response of a channel to external stimuli. For example,

pH changes can stimulate the transition between swollen and collapsed states of pH-responsive molecules which vary the degree of rectification.[93] Temperature change can also be sensed by ICR through incorporation of amine-terminated polymer brushes inside conical nanopores that shrink or swell with changing temperature.[94] As previously demonstrated in glass nanopores,[95] PET nanopores are gated optically by irradiating photolabile protecting groups with UV light.[96]

Nanostructures functionalized with different molecules at opposite ends are able to tune transport. Conical nanopores modified with DNA oligomers exhibit both reversible voltage and pH gating and have extraordinarily high rectification at high pH.[97] Similarly, pH-dependent rectification is enhanced by hydrophobic C10 and C18 thiol gates on one side of a nanopore due to the increased resistance of the hydrophobic layer.[98] pH- and light-responsive nanochannels are realized by modification with dual-responsive malachite[99] or spiropyran[100] molecules (Figure 2b). Cigar-shaped nanochannels modified at opposite ends by different molecules act as double-gated ion pumps.[93,101] A smart homopolymer that is both pH and temperature sensitive produces reversible switching of rectification in glass nanopores.[102] C4-DNA motors attached to PET pores change conformation by accepting or releasing protons generated indirectly by UV irradiation of a photo-

induced OH^- emitter, malachite green carbinol base (MGCB), and adsorb cetyltrimethylammonium bromide (CTAB) molecules that physically block the pore.[103] UV exposure causes an increase in pH which, in turn, causes the DNA motors to stretch to a single-stranded structure that can adsorb more blockers and effectively reduce current compared to DNA motors at low pH that form a shorter, i-motif structure with fewer adsorbed blockers. Asymmetric surface charge distribution is established in highly ordered nanochannel arrays in porous anodic alumina membranes by functionalizing the surface with amine groups to induce pH-dependent ICR.[104]

Modification of nanopore surfaces also permits nanoscale sensing. Calcein-modified channels bind calcium ions, which reduce conductance in the high-conductance state.[105] Similarly, lactoferrin is also sensed by nanopores modified with iron-terpyridine.[106] PET pores modified with β-cyclodextrin discriminate between enantiomers of histidine.[107] Interestingly, L-histidine selectively binds to the β-cyclodextrin, leading to an increase in the rectification ratio, but D-histidine does not interact with the host molecule, resulting in no change. Rectification also occurs in structures with symmetric pore geometries and uniform charge distributions when a nanoparticle partially blocks the pore entrance, and direction of rectification depends on the charge of both the functionalized polystyrene particle and pore.[108] Concentration gradients of the electrolyte influence rectification ratios due to cooperation and competition between geometry-induced asymmetric transport and diffusive ion flow.[109] A switch from a high-conductance state to a low-conductance state occurs over a very short, tunable voltage window (10 mV) for nanopores separating a low conductivity solution from a high conductivity solution due to negative differential electrolyte resistance and bistable fluid flow.[110,111] As an externally applied pressure increases, the potential at which a ~80% decrease in current is observed becomes more negative. Pressure-driven flow disrupts cation and anion distributions in and adjacent to nanopores and can eliminate ICR in large nanopores (~200 nm radii) but has a negligible effect on pores with radii below 30 nm.[112]

In small nanopores (3−25 nm in diameter), the size of monovalent cations impacts the degree of current rectification. Figure 2c shows that experimental results are in good agreement with simulations and that rectification increases with increasing cation size for these small pores.[113] Simulations of current flow in weakly selective pores suggest that intrapore depletion and enrichment zones are responsible for ICR and that inversion of rectification is possible.[114] However, in highly selective pores, concentration depletion external to the pore leads to rectification, and rectification inversion is possible at high applied voltages. Another theoretical model suggests that diode-like current behavior is possible in the presence of a concentration gradient, and ion selectivity may be reversed if the gradient is high enough.[89] Functionalization of nanostructures in close proximity to nanopores alters their rectification behavior. Modification of the outer membrane of neutral nanopores with polyelectrolyte varies the current rectification and has also been modeled.[68,115] This modification is advantageous for multiple reasons, including easier access of outer membranes to modification and enhanced rectification due to the immobilized surface charge. Theoretical work suggests that gating performance and modulation of conductance states by field effect modulation of the zeta potential is higher when the background electrolyte concentration and pH are both low.[116]

Nanopipets exhibit ICR when the tip of the pipet is similar in dimension to the Debye length[117] or the tip is blocked by a charged surface. Current rectification is reversible in quartz nanopipets that are modified by immersing the pipet in a saccharide-binding polymer.[118] High- and low-conductance states that correlate to the collapse and swelling of the polymer are switched in the presence of saccharide or changes in pH. The direction of rectification in nanopipets is also reversed by modification of the surface with poly(ethylene imine) (PEI), a positively charged polymer,[119,120] and the magnitude of rectification depends on electrolyte concentration.[121] PEI-modified pores decorated with glucose oxidase reverse the direction of rectification again and reduce $AlCl_4^-$ ions.[119] Similarly, a chitosan-modified nanopipet detects changes in ICR that correlate to binding of Cu^{2+} and obtain the associated binding affinity of the ion.[122]

For nanopipets, ICR is affected by the tip diameter, surface charge of the tip,[85,123] and cone angle of the pipet.[124] When nanopipets are in close proximity to a charged surface, the ICR can also be influenced.[125−127] This effect distinguishes cationic and anionic substrates through the observation of ICR changes in a pipet held tens to hundreds of nanometers from the surface.[127] This study is further supported by finite element simulations (Figure 2e).[128] Other studies describe conditions in which current is enhanced as a pipet approaches a surface due to electroosmotic flow separation.[125] A substrate with a surface charge density 10-fold higher than a pipet dominates and dictates ICR instead of the pipet. The interplay between the pipet and surface is seen in simultaneous topographic measurements and substrate surface charge mapping by SICM.[126] In these studies, ac techniques enhance the determination of surface charge and provide additional insight into nanoscale interfacial chemistry.

Nanofluidic Diodes and Transistors. Asymmetric current flow in nanofluidic devices is analogous to the behavior of electronic diodes[129] and transistors[130] with the exception that ions in solution rather than electrons act as the charge carriers.[131] Embedded electrodes in nanochannels and concentration gradients near a nanofluidic structure act as a controllable gate to effectively alter current flow through the channel.

A cylindrical thermosensitive channel is formed with triblock copolymer brushes whose configuration and phase behavior depend on temperature.[132] Closed channels are opened by increased temperature until a threshold temperature is reached, and further increases in temperature cause the channels to reclose. Bipolar membranes also exhibit nonlinear current behavior in a process similar to PN-junctions in electronic transistors. Use of polyphosphonium as a polycation in bipolar membrane diodes allows a large window of usable gate voltages.[133] Stacking of bipolar membranes in series suppresses ion accumulation, produces faster off-switching with reduced hysteresis, and forms a fluidic AND gate.[134] Simulations of diode-like pores conclude that ICR is solution-dependent, and a maximum in ICR is observed due to the balance between increased ion enrichment inside the pore and depletion outside the reservoir.[129]

Addition of a concentration gradient acts as a gate electrode near the nanostructure and modulates voltage, which, in turn, influences fluid transport and ICR. Electrostatic gating of nanochannels by tuned gradients in ionic strength controls the release of fullerene derivatives.[135] Voltages applied to a gate electrode adjacent to a nanochannel dictate the degree of
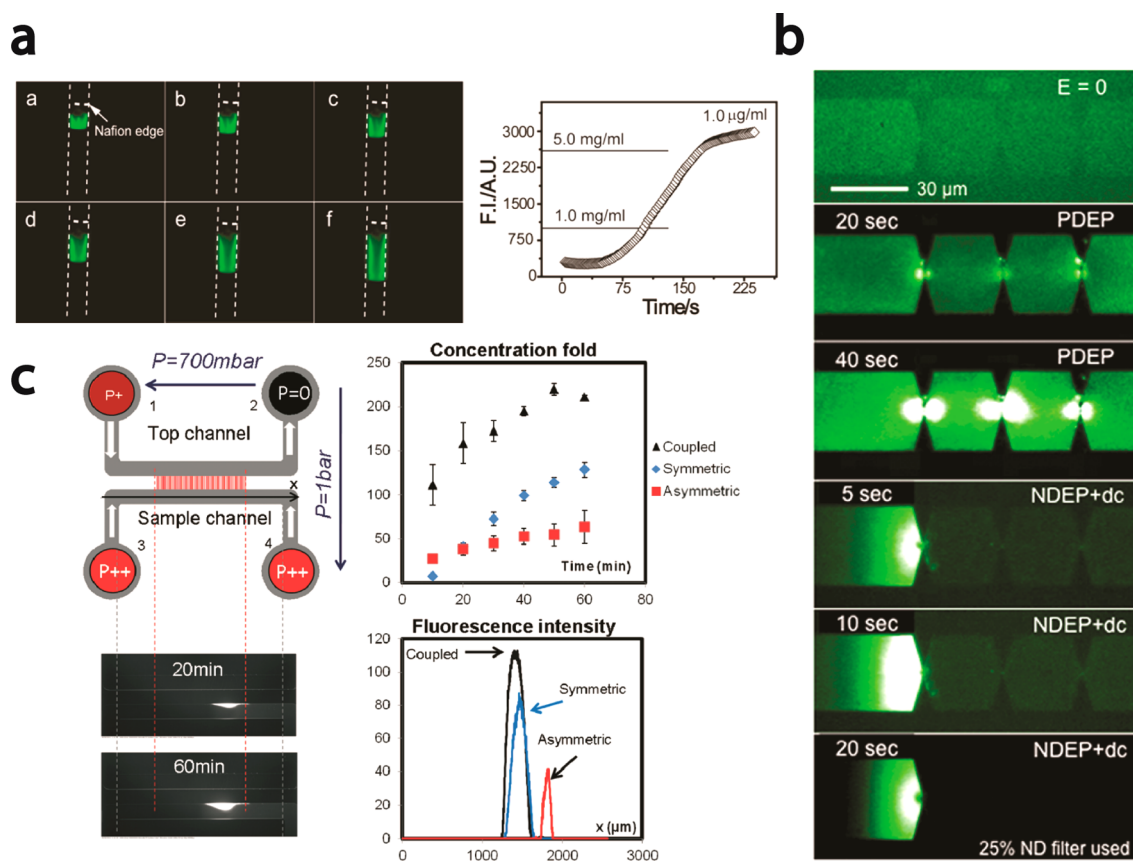
Figure 3. Sample enrichment at junctions between micro- and nanochannels occurs when there is preferential ion transport. (a) A nanoporous membrane integrated in a microchannel produces an enrichment region that increases with time. Reprinted from ref 151. Copyright 2014 American Chemical Society. (b) Nanoconstrictions along a nanochannel concentrate fluorescently tagged proteins by electrodeless dielectrophoresis. Reprinted from ref 154. Copyright 2012 American Chemical Society. (c) Pressure-driven flow concentrates fluorescent nanobeads in a bypass micro- and nanofluidic device. Reprinted from ref 155 with permission of The Royal Society of Chemistry. Copyright 2013 The Royal Society of Chemistry.

rectification within the nanochannel.[136] Biasing potentials less than 1 V applied through metal gate electrodes control the capture of DNA in 200 nm pores.[137] A potential applied to a gate electrode embedded in a nanochannel is simulated and predicts that surface charge density becomes more negative with increasing potential, resulting in increased EOF.[72,138] Additional simulations show that gated nanochannels exhibit enrichment and depletion, depending on the polarity of the surface charge and applied gate potential.[139] Simulations of changes in surface charge density of gated nanopores suggest that modulation in pore conductance is dependent on pH, ionic strength, and applied voltage.[140]

Theoretical and experimental results with a three-electrode nanopore show changes in the electric field induced by a working electrode adjacent to a nanopore leads to ICR at high salt concentrations.[141] Active gating of semiconducting nanopores significantly enhances rectification ratios.[24] Heterostructured FET-like arrays tune ICR through modulation of the potential applied to a metal gate near the nanopore array.[92] Two conical nanopores aligned in parallel or series can also function as a gating network.[142] Rectification depends on the orientation of both pores and direction of the applied potential. Branched alumina nanochannels act like tunable nanofluidic diodes due to the cooperative asymmetry of the branched structure.[143]

Concentration Polarization and Sample Enrichment. Uneven ion flux and emergence of concentration gradients

occur when potentials are applied across microchannel-nanochannel junctions. When the electrophoretic mobility of ions is greater than diffusive transport in the adjacent microchannels, counterions are depleted on the feed side of the nanochannel due to preferential transport through the charged channel and accumulate on the other side. Simultaneously, co-ion transport through the same channel is hindered, and concentration polarization (CP) results.[144] Charged molecules are enriched by the CP mechanism, and preconcentration of limited samples is possible. If the electroosmotic and electrophoretic forces are balanced, sample stacking can occur at the boundary of the depletion region, away from the micro- and nanochannel junction.[145]

Closed, elastomeric valves in PDMS devices act as nanoscale conduits and can induce CP effects.[146] Such a device generates 10^3-fold preconcentration of fluorescein in a 2 mM lithium carbonate solution in ~270 s with a single channel. Nanoporous membranes efficiently concentrate samples. Embedded nanoporous membranes in nanofluidic paper devices enrich a fluorescent tracer by 40-fold,[147] and nanofractures formed by nanoparticle-assisted electric breakdown between two microchannels concentrate a protein sample 10^4-fold in 60 min.[148] Polyacrylamide gels integrated into microchannels form a micro- and nanochannel junction that yields 600-fold enrichment within 120 s.[149] Controlled hydrodynamic flow adjacent to a Nafion nanojunction membrane limits the propagation of CP by continuously replenishing charge carriers to the
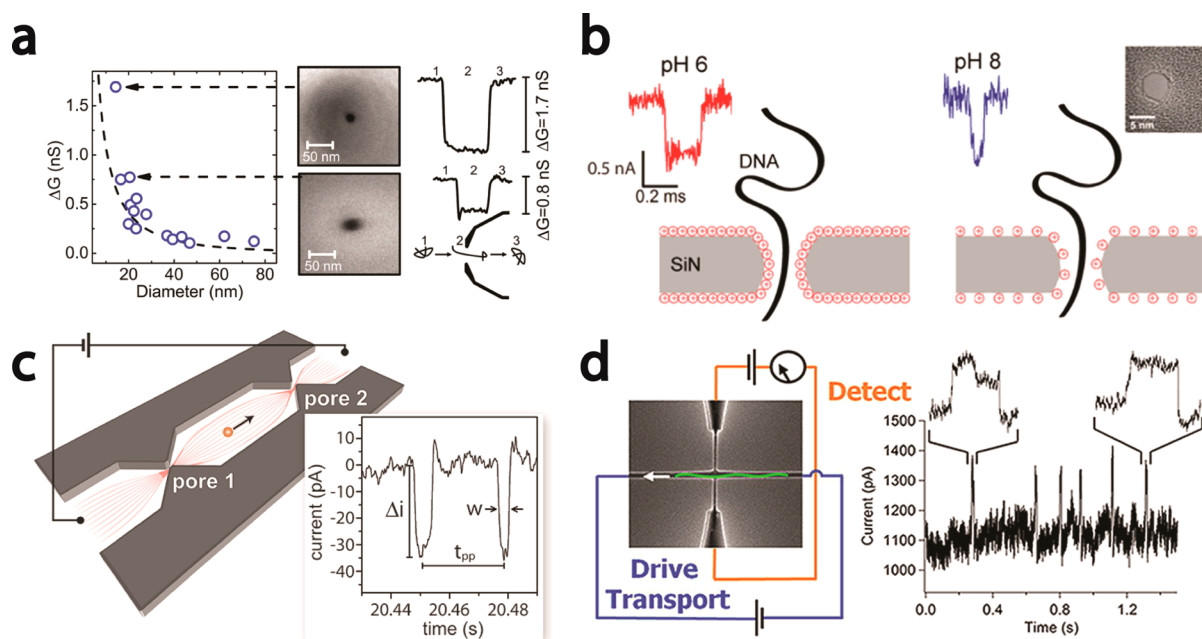
Figure 4. Resistive-pulse sensing in nanoscale conduits with dimensions comparable to the size of the analyte of interest. (a) Nanopipets sense DNA molecules with increasing sensitivity as pore diameter is reduced. Reprinted from ref 166. Copyright 2013 American Chemical Society. (b) DNA translocates through amine-functionalized nanopores, and translocation time through the pore depends on the surface-charge density, which is tuned by pH. Reprinted with permission from ref 191. Copyright 2013 American Chemical Society. (c) In-plane nanochannel with two pores in series detects each hepatitis B virus particle twice during transit through the nanochannel. Reprinted from ref 32. Copyright 2011 American Chemical Society. (d) DNA driven through a long nanochannel in a glass substrate is detected electrically as the DNA passes a shorter, lateral nanochannel. Reprinted from ref 38. Copyright 2012 American Chemical Society.

depletion region and confining the CP region to a triangular region near the junction.[150] At high hydrodynamic inflows, the limiting-current region is eliminated, which results in increased power efficiency. Moreover, enzyme activity increases in regions of enriched targets. Figure 3a shows the preconcentration of quenched, dye-labeled nanoparticles concentrated near a Nafion membrane.[151] Trypsin molecules in solution cleave proteins bound to the nanoparticles, and the cleaved proteins fluoresce. In another example, a Nafion membrane is cast in a microfracture region[23] as a microfabrication-free technique to electrokinetically stack and enrich DNA.[152]

Regions of cathodic and anodic focusing occur in the same glass-nanoslit structures by hydrostatic-pressure stabilization of CP effects.[153] Dielectric nanoconstrictions embedded in nanofluidic devices act as field-focusing lenses that generate molecular traps and dams by dielectrophoresis for rapid protein enrichment (Figure 3b).[154] Figure 3c shows electroless preconcentration in silicon nanofluidic devices with a symmetric pressure-driven crossflow to concentrate particles at a discrete point. In the same device, an asymmetric pressure-driven mode generates a streaming potential[155] and concentrates *E. coli* bacteria 50-fold in only 40 s. Proteins are enriched in nanochannels with a pH gradient along the length of the channel by balancing the forces of pH-dependent charge and viscous drag.[156] Alternatively, proteins are focused at different ends of a nanochannel by concentration gradient focusing.[157,158]

The nonlinear voltage behavior associated with CP is affected by pH.[159] A microfluidic device with a photopolymerized, nanoporous polyacrylamide membrane has pH fluctuations >1.5 pH units, which are mapped spatiotemporally and depend strongly on buffer properties.[160] Three-dimensional numerical simulations of a nanofunnel positioned between two straight

nanochannels indicate that enrichment and depletion zones propagate away from the nanofunnel in a high-conductance state but remain localized in a low-conductance state.[161] Simulations of CP development and vortex generation also found that the electrophoretic mobilities of counterions in a nanoporous membrane affect CP, i.e., CP strength increases with counterion mobility. Moreover, preconcentration increases with increasing electric potentials that generate vortex flow and a slow-flow zone near the membrane.[162]

Resistive-Pulse Sensing. Nanofluidic devices with critical dimensions comparable to the size of a particle can be used for resistive-pulse sensing (RPS), which is a label-free, non-destructive method to detect individual particles. Transient reductions in ion current, or pulses, occur when particles pass through an electrically biased conduit and are proportional to particle size. Conduit dimensions are tuned to detect specific particle sizes, and the ability to readily manufacture nanoscale features has increased the types of nanoscale particles that can be sensed. This technique is of particular interest as a means of rapid genomic sequencing.[163−165] Resistive-pulse experiments can be categorized as in-plane or out-of-plane depending on device orientation and particle motion. Out-of-plane devices incorporate nanopores perpendicular to the substrate surface whereas in-plane devices have nanopores fabricated parallel to the substrate surface.

Pulse characteristics encode information about particle and pore geometry as well as information about interactions between the analyte and pore. Particle size relative to the pore dimensions dictates the amplitude of a current pulse, and pores can be modified to better match particle size and increase pulse amplitude. Figure 4a shows that decreasing pore diameters produce larger changes in conductance.[166] Particles of unknown sizes are measured with nanopores calibrated with

particles of known sizes.[167] Pores fabricated in ultrathin silicon nitride membranes characterize the binding of a drug or molecule to an RNA complex by measuring differences in pulse amplitude for bound and unbound molecules.[168] Monitoring bare and bound antibodies produce similar changes in current.[169]

Interactions between particles and nanopores produce pulses with variable widths and may be electrostatic or size-based in nature. Pulse shapes depend on the shape of the constriction,[170] and the effect of pore geometry on pulse shape[171] as well as deformation of hydrogel particles within the pore[172] are studied with PET nanopores. The size, charge, and zeta potential of translocating particles can also be extracted from pulse width.[173−176] The surface charge of nanoparticles is also measured by applying pressure across a nanopore to oppose electrokinetic flow.[177,178] When the opposing pressure completely counteracts the electrokinetic flow, the particle velocity is zero, and current pulses are not observed. Pore sculpting alters the shape of drilled nanopores and has a direct impact on pulse shape, i.e., pores drilled directly by an ion beam have smaller average diameters than pores sculpted to the same critical dimension by an ion beam.[21] Larger average diameters of the sculpted pores result in lower pulse amplitudes, and longer translocation times occur in the case of the e-beam sculpted pores. Biological pores are capable of detecting trace levels of cocaine by binding drug molecules to DNA aptamers that become lodged in the pore and cause an extended current blockage.[179]

Longer DNA molecules have longer translocation times compared to shorter DNA molecules in a fixed-length nanochannel, and an asymmetric bipolar pulse leads to rapid separation of different-length molecules.[180] Binding of proteins to DNA aptamers immobilized on nanobeads show increased pulse widths.[181] Deformable channels with reduced cross sections generate DNA-translocation events with reduced frequency and longer pulse widths.[182] The buffer pH can cause nanoparticles to expand, and swollen particles are forced to squeeze through the pore, resulting in increased pulse widths.[183] When bovine serum albumin (BSA) molecules in various conformations pass through a TEM-drilled nanopore and are detected electrically,[10] the denatured forms of BSA produce wider pulse widths than nondenatured BSA because of increased interactions with the pore walls. Carboxylate-modified polystyrene spheres create asymmetric pulses passing through size-tunable nanopores, and pulse-shape is particle-size dependent.[184]

Understanding the processes by which particles enter nanoscale constrictions and how the particles behave while inside a constriction is critical to designing devices with optimized performance. Access resistance dominates particle translocation and barely fluctuates during particle translocation.[185] In pore-cavity-pore devices, nanoscale confinement in single-particle data suggests a narrow escape, whereas ensemble measurements suggest crowding effects, which drive escape even at low particle concentration.[186] The motion of fluorescent DNA is visualized and affected by both electro-osmosis and electrophoresis, and capture volumes for small nanopores are calculated by finite element simulations.[187]

Coating of nanopores increases the functionality and reliability of nanopore sensors. Nanopores coated with a fluid lipid bilayer mimic biological pores, and the coating minimizes clogging and nonspecific binding as well as reduces translocation times.[188,189] Chemical modification of PET membranes with triethylene glycol suppresses electroosmotic flow and minimizes particle adsorption for characterization of hepatitis B virus capsids.[190] Figure 4b shows the difference in pulse widths for pores coated with 3-aminopropyltrimethoxy-silane (APTMS) and surface charge tuned with pH.[191] As pH is increased from 6 to 8, surface charge density is reduced and translocation times for DNA decrease.

RPS devices fabricated in-plane have the added advantages of incorporation of multiple sensors in series as well as optical monitoring to better understand transport through a device. Figure 4c shows a nanochannel with two nanopores in series for detection of hepatitis B virus capsids, and the pore-to-pore transit time is used to determine the electrophoretic mobility of the capsids.[32] A pulse is recorded each time a capsid passes through a pore, and a pulse pair corresponds to a single capsid passing through the two pores in series. With a different in-plane design, electrodes with a nanoscale gap embedded in a nanopore detect and count metal-encapsulated fullerenes and DNA oligomers.[192] Lateral conductance measurements of dsDNA molecules in a long nanochannel are made through shorter channels positioned perpendicular to the translocation channel (Figure 4d).[38] Measurements of electrophoretic mobility and optical detection of molecules are possible in this design, and measuring current in a shorter channel produces higher signal-to-noise ratios by minimizing the potential dropped along the channel. Another in-plane method uses geometric nodes distributed along a nanochannel to produce pulse shapes with distinct current signatures.[193] This design senses the presence of particles even when the signal-to-noise ratios are low, as demonstrated by the detection of HIV in human plasma. Simultaneous optical and electrical sensing of single particles combines particle tracking and unambiguous detection of fluorescently labeled beads at the nanoconstrictions in an in-plane nanochannel with adjacent electrodes.[194]

Rapid and cost-effective sequencing of DNA may be possible with RPS through electrical discrimination of individual DNA bases. Molecular dynamics simulations suggest that tunneling currents through all four DNA bases are statistically different and that transverse sensing of translocating DNA molecules can discriminate among the bases.[195] FIB-milled nanopores with integrated tunneling electrodes are used to detect DNA molecules by both tunneling current and ion current.[15] Nanopores milled in graphene nanoribbons also detect DNA translocation with a relatively slow translocation speed.[196] Simulations of molecularly thin graphene nanogaps predict that the four bases are distinguished by their electrical tunneling currents.[197] Ion conductance through the pore and electrical conductance through the graphene are measured simultaneously and are altered when a particle passes through the pore. Devices consisting of silicon nanowires adjacent to a nanopore act as FET sensors to detect the translocation of DNA molecules.[198] FET conductance and ionic current are recorded simultaneously and may be used for DNA sequencing in the future. Two nanopores stacked in series can estimate the electrophoretic mobility of DNA molecules by measuring the time-of-flight between pores.[199] Transport of DNA molecules passing through a nanoconstriction depends on the shape of the constriction. Simulations with graphene as the sensing substrate predict that nanopores drilled through a graphene monolayer with zigzag edges have significantly enhanced current signals when DNA translocates through the pore.[200]

Resistive-pulse sensing with conical nanopores in nanopipets and glass membranes has an advantage over cylindrical

nanopores because the direction of particle translocation can be extracted from the asymmetric pulse shape produced by conical pores.[201] This phenomenon is attributed to a nonuniform electric field within the pore. Current pulses observed during particle translocation transition from a single-peak pulse to a biphasic pulse consisting of an increased current peak before the current decreases at high negative potentials (<−0.4 V).[202] The biphasic nature of the pulse is a result of increased conductivity from the surface charge of the translocating particle and the displacement of ionic solution within the pore.

Efforts to make RPS more quantitative have been directed toward evaluation of solution concentration by correlating the current blockage event and diffusion current of the particle to the orifice.[203−205] The effect of salt concentration on the translocation of DNA through quartz nanopipets demonstrate that at high salt concentrations translocation events result in a decrease in current, but at low salt concentrations, DNA translocation actually increases the ionic current.[206] Label-free in-flow detection of single DNA[207] and protein[208] molecules is possible as molecules pass by the nanopipet tip. Also, there are efforts to use the peak shape and exploit the surface charge on the nanopores to sense charged analytes bound to a nanoparticle surface. Resistive-pulse sensing distinguishes between peptide-modified particles and antibodies attached to these peptide-modified particles.[205] Current pulses produced by antibody-conjugated particles and bare Au or Au-peptide nanoparticles occur at potentials with opposite polarity and are oriented in opposite directions, which enables selective detection of antibodies.

Nanofluidic Separations and Sieving. Molecular separations in nanochannel devices are of considerable interest for rapidly sorting and sensing particles. Several nanofluidic mechanisms are used to separate molecules with improved resolution and separation speed as well as separation of nanometer-sized particles. Particles are often separated by size, length, or charge, and sieving structures are tailored to exploit these differences.

Arrays with nanoscale step heights fractionate protein samples based on size.[209] Flow-counterbalanced capillary electrophoresis uses periodic pressure-driven backflow to generate uneven EOF at a micro- and nanofluidic channel junction to execute charge-based separations with significantly reduced separation lengths.[74] Shear-driven flow generates high flow velocities for high-speed chromatographic separations of two fluorescent molecules in nanochannels.[210] Zeptomole concentrations of nonfluorescent dye molecules are chromatographically separated in a nanofluidic channels and detected by differential interference contrast thermal lens microscopy (DIC-TLM).[211,212] Molecules are selectively transported through intrinsic defects in graphene by pressure and diffusion and filtered by size.[213] Voltage-tuned nanopores are modeled with Brownian dynamics and are predicted to filter nanoparticles by altering the local electric field within the pore.[214] Modeling also shows that nanochannels with finite EDLs and added pressure-driven flow separate ions with the same electrophoretic mobility but different valence.[215] In addition, modeling of nanoparticle separations through a nanopore shows that EOF significantly impacts separation and can be tailored to make pores permeable to only one type of particle.[216] Proteins are isolated at different ends of a nanochannel by concentration gradient focusing, and theoretical data are in good agreement with experimental data.[157,158]

A sieving structure composed of a nanoslit formed between a bowed ridge and a coverslip is used for fast and continuous separation of nanoparticles[217] and DNA complexes.[218] Small analyte molecules pass through the nanoslit unhindered, whereas larger molecules are trapped at the ridge and must find alternative pathways. DNA is rapidly sieved with cylindrical glass capillaries at high applied voltages.[219] The effects of ionic strength on the separation of single-stranded and double-stranded DNA are probed in glass nanochannels.[220] Electrophoretic mobilities shift at different ionic strengths, and the mobility difference between ss- and dsDNA increases as ionic strength increases. DNA molecules of different lengths are also separated in nanochannels with an asymmetric bipolar pulse.[180] Shorter molecules migrate completely through the channel during the forward bias of the asymmetric pulse, whereas longer molecules do not transit the entire channel and are pulled back during the reverse bias. Simulations of Brownian dynamics of DNA translocation through nanofilter arrays support experimental results of variable pathways according to DNA length.[221]

Small Volume Delivery/Manipulation. Handling of ultrasmall volumes of liquid is critical to many analytical techniques. Nanofluidic structures easily handle and store small sample volumes, and electrokinetic transport can precisely manipulate attoliter-scale fluid volumes.[222] Liquid flow rates in the pL/min regime are monitored in nanochannels by detection of electrochemically active molecules with electrical cross-correlation spectroscopy.[223] A Laplace nanovalve generates 1.7 fL water droplets in air, and these droplets are controlled in a nanochannel.[224]

Nanopipets provide a straightforward route to manipulate nano- to attoliter volumes of fluids. Electroosmotic transport delivers small volumes of fluids from nanopipets, which can be used to inject cells.[225] Deposition and delivery of molecules by nanopipets have been explored widely for about a decade, but quantitative data of amounts dispensed are lacking. A carbon ring/nanopore electrode at the tip of nanopipet quantitatively estimates the amount of charged molecules delivered.[226] These studies reveal the impact (enhanced or diminished delivery) of nanopipet surface charge on delivery of charged molecules by electroosmosis. Finite element simulations and theoretical studies determine the effects of pipet size, delivery voltage, pressure, and distance to the underlying substrate on the spatial distribution of delivered molecules.[227] Moreover, understanding the role of each parameter (pipet size, pressure and voltage, and distance between probe and substrate) on delivery enables development of a robust methodology for quantitative and localized drug delivery.

Fluid aspiration with nanopipets allows sampling and dispensing of attoliter to picoliter volumes of fluid by application of voltage across a liquid−liquid interface.[228] Changes in the surface tension at the interface, as a result of application of voltage, generate forces sufficient to aspirate and dispense fluids.[229] This method selectively extracted mitochondrial DNA from single human BJ fibroblast cells, and sequencing characterized the aspirated mitochondrial DNA. EOF through nanopipets can also deposit and inject dyes[225,230] and microparticles.[231] An electric field generated between electrodes in each barrel of a theta pipet controls the electromigration of charged microparticles between the two barrels through a thin liquid meniscus between the substrate and pipet.[231] Substrate charge affects the deposition rate of charged microparticles with higher deposition rates for surfaces
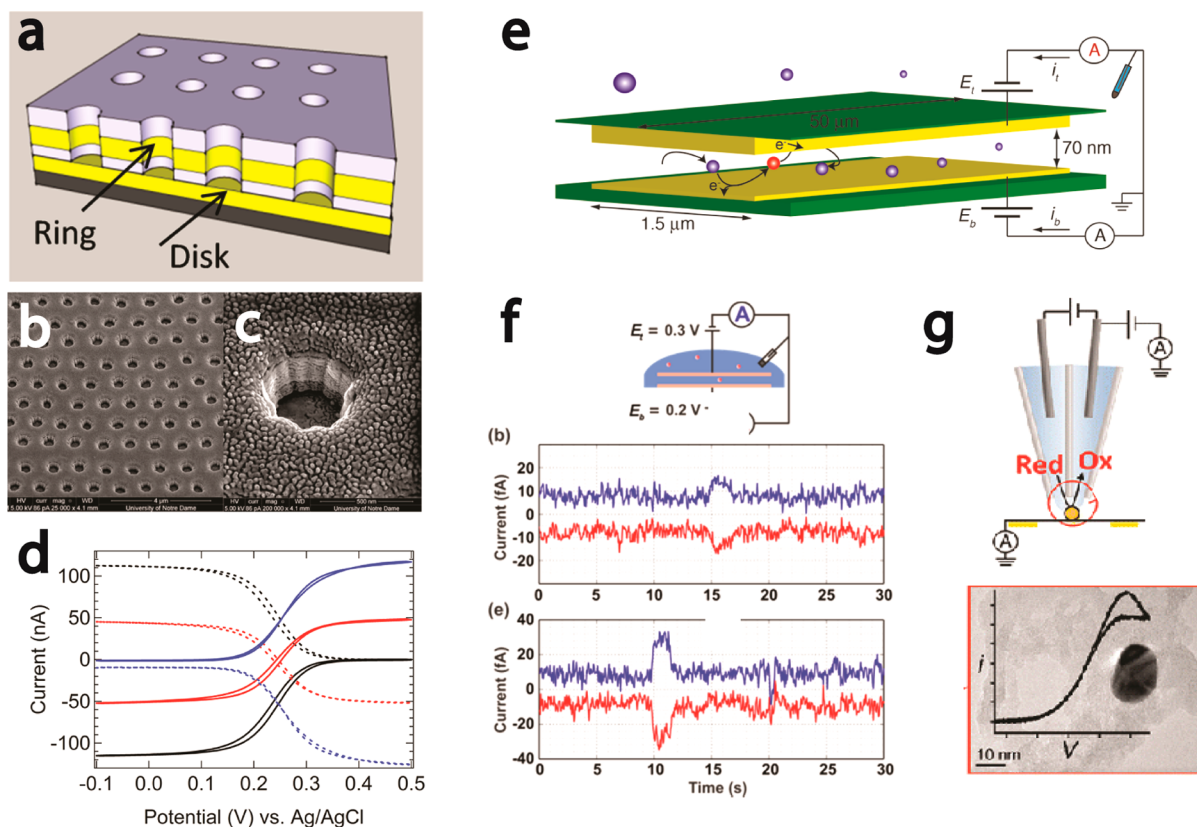
Figure 5. Electrochemical reactions conducted in nanofluidic devices offer increased efficiency and enable single-particle reactions. (a−d) Nanoscale ring-disk electrodes fabricated by FIB milling exhibit enhanced molecular transport and current density compared to microscale devices. Reprinted from ref 241. Copyright 2013 American Chemical Society. (e) Nanogap transducers act as stochastic sensors and have sufficient gain to track the reduction of single particles. Reprinted from ref 238. Copyright 2011 American Chemical Society. (f) Single-molecule events measured in nanogap transducers are detected as discrete current steps. Reprinted from ref 240. Copyright 2013 American Chemical Society. (g) Nanoscale droplets formed at an electrode−surface interface act as electrochemical cells to measure the electrocatalytic activity of single gold nanoparticles. Reprinted from ref 247. Copyright 2012 American Chemical Society.

with like charge, and the pipet successfully delivered particles inside individual *Zea mays* root hair cells.

Nanoscale Electrochemistry. Several types of electrochemical reactions are monitored by nanofluidic devices.[232] Electrolysis of water is conducted experimentally in nanochannels and theoretically modeled.[233] The emission intensity of pH-dependent fluorescein tracks production of H_2. Figure 5a−d shows annular metal electrodes embedded in nanocapillary arrays that act as working electrodes for electrochemical conversion.[234] Reagent delivery is enhanced by EOF, and conversion efficiency in these nanoarrays is an order of magnitude greater than in microscale structures. Simulations of transport in these nanoband arrays predict that transport of reacted species away from the reaction site is much faster in nanochannels than in microchannels due to rapid diffusion away from the center of the nanopore.[235] Isoelectric points of bound proteins are determined from the transport rate of ferricyanide through protein-modified PAA nanochannels at different pH levels.[236]

Single-molecule detection platforms provide a method to study and understand the response of a molecule to a particular environment without perturbation from adjacent molecules.[237] To study single molecules in nanofluidic structures, a small number of molecules are trapped in a nanogap between parallel electrodes (Figure 5e)[238] to measure the oxidation and reduction of redox molecules (Figure 5f).[239,240] The molecules rapidly diffuse between the two electrodes and are subjected to

multiple cycles of oxidation and reduction to achieve the desired current amplification.[241] This technique was first used to study single molecules by an electrochemical method,[242] and the same concept was adopted by several groups, who employ more well-defined designs with parallel electrodes[243] and nanofluidic channels.[240,241,244] Simulations looked at the noise associated with redox-sensors and determined that concentration fluctuations and adsorption contribute to observed noise effects.[245,246] Nanopipets use a similar strategy to confine a small number of molecules or particles in a small gap. The liquid meniscus formed between a nanopipet and a conductive substrate behaves like a small electrochemical cell (the area of the electrode is a few micrometers squared). Confinement of a small number of particles enables investigation of the electrocatalytic activity of individual gold nanoparticles.[247] Figure 5g shows a schematic of meniscus formation at the pipet-surface interface and a typical $i–V$ curve for a single gold nanoparticle on the electrode surface.

Electrospray Ionization. Nanopipets with tip diameters <100 nm (Figure 1e) can be used as electrospray emitters and coupled to a mass spectrometer.[248] The resulting mass spectra exhibit a number of interesting features such as a reduced number of charged states for all of the large analytes and a shift toward peaks with higher charged states, which may be a consequence of formation of droplets having high surface charge density. Further, samples sprayed from nanopipets have a greater signal-to-noise ratio compared to samples sprayed

from commercial pico-tips. Detailed characterization of the nanopipet tips before and after ESI confirms the robustness of these tips under ESI conditions. This methodology is particularly attractive for imaging studies that make use of the small tip size.

OUTLOOK

Nanofluidics has experienced significant growth in the past two decades, driven primarily by fundamental studies of physical forces in nanoscale conduits and a better understanding how these forces uniquely impact ion and fluid transport at the nanoscale. Interest in nanofluidics continues to grow with improved fabrication techniques that generate even smaller critical dimensions with higher precision and repeatability. Future work with nanofluidic devices will include fundamental studies of nanoscale transport to improve device performance and application of nanofluidic devices to a wider range of analytical problems. Of particular interest is the prospect of nanopore devices to sequence DNA, which has, and will continue to be, a top priority in nanofluidic research.

To achieve these goals, fundamental challenges facing nanofluidic research must be addressed, despite the recent introduction of commercially available sequencing devices.[249,250] A major challenge facing the field of nanofluidics is the lack of high-throughput, cost-effective nanofabrication techniques with high device-to-device reproducibility. Fabrication and testing of these devices are typically confined to academic laboratories because expensive equipment and significant fabrication time make scaled-up production of commercial instruments difficult. In addition to fabrication constraints, most nanofluidic devices require sophisticated support electronics with sufficient current amplification and noise reduction to achieve high signal-to-noise ratios for the analytes of interest. Engineering devices with quiet, high-speed electronics and fast data analysis will be an important next step to transition nanofluidic devices from the laboratory to everyday use. Despite these limitations, nanofluidic research will continue to expand our understanding of fundamental transport phenomena and improve analytical methods.

AUTHOR INFORMATION

Corresponding Authors
*E-mail: lanbaker@indiana.edu.
*E-mail: jacobson@indiana.edu.
Notes
The authors declare no competing financial interest.
Biographies
Daniel G. Haywood received his B.S. in chemistry in 2011 from Hope College in Holland, Michigan. He is currently a graduate student in the Department of Chemistry at Indiana University-Bloomington in Stephen Jacobson's laboratory and is investigating fundamental nanofluidic transport and biological applications of nanofluidic sensing.

Anumita Saha-Shah received her B.S. and M.S. in chemistry from University of Calcutta in 2007 and 2009, respectively, followed by a brief research experience at Unilever Industries Pvt Ltd. working as a research executive. She is currently a graduate student in the Department of Chemistry at Indiana University in Lane Baker's laboratory and is investigating small volume fluid manipulation techniques to interface with mass spectrometry.

Lane A. Baker received a B.S. degree from Missouri State University in 1996. He was awarded his Ph.D. degree at Texas A&M University in 2001. He completed a National Research Council Postdoctoral Associateship at the Naval Research Laboratory in Washington, DC, in addition to a postdoctoral appointment at the University of Florida. His current research interests include electrochemical methods for analysis and imaging, and work in his group is focused on applications of nanopores for the development of chemically and biochemically selective membranes, sensor development, and electrochemical imaging.

Stephen C. Jacobson received a B.S. in mathematics from Georgetown University in 1988 and a Ph.D. in chemistry from the University of Tennessee in 1992. After graduate school, he was awarded an Alexander Hollaender Distinguished Postdoctoral Fellowship at Oak Ridge National Laboratory (ORNL), and in 1995, he became a research staff member at ORNL. In 2003, he joined the faculty at Indiana University and is currently a professor in the Department of Chemistry. Research in the Jacobson group is directed toward miniaturization of analytical instrumentation with an emphasis on micro- and nanofluidic devices. His research group is currently working in the areas of microfluidic separations, nanofluidic transport, cancer screening, virus sensing, and bacterial adhesion and aging.

ACKNOWLEDGMENTS

REFERENCES

(1) Schoch, R.; Han, J.; Renaud, P. *Rev. Mod. Phys.* **2008**, *80*, 839−883.
(2) Zhou, K.; Perry, J. M.; Jacobson, S. C. *Annu. Rev. Anal. Chem.* **2011**, *4*, 321−41.
(3) Chen, X.; Xu, B. X.; Liu, L. *Appl. Mech. Rev.* **2014**, *66*, 050803.
(4) Prakash, S.; Pinti, M.; Bhushan, B. *Philos. Trans. A Math Phys. Eng. Sci.* **2012**, *370*, 2269−303.
(5) Park, H. G.; Jung, Y. *Chem. Soc. Rev.* **2014**, *43*, 565−576.
(6) Jiang, L. L.; Fan, Z. J. *Nanoscale* **2014**, *6*, 1922−1945.
(7) Xia, Y. N.; Yang, P. D.; Sun, Y. G.; Wu, Y. Y.; Mayers, B.; Gates, B.; Yin, Y. D.; Kim, F.; Yan, Y. Q. *Adv. Mater.* **2003**, *15*, 353−389.
(8) Duan, C.; Wang, W.; Xie, Q. *Biomicrofluidics* **2013**, *7*, 26501.
(9) Mijatovic, D.; Eijkel, J. C. T.; van den Berg, A. *Lab Chip* **2005**, *5*, 492−500.
(10) Freedman, K. J.; Jurgens, M.; Prabhu, A.; Ahn, C. W.; Jemth, P.; Edel, J. B.; Kim, M. J. *Anal. Chem.* **2011**, *83*, 5137−5144.
(11) Fanget, A.; Traversi, F.; Khlybov, S.; Granjon, P.; Magrez, A.; Forro, L.; Radenovic, A. *Nano Lett.* **2014**, *14*, 244−249.
(12) Healy, K.; Ray, V.; Willis, L. J.; Peterman, N.; Bartel, J.; Drndic, M. *Electrophoresis* **2012**, *33*, 3488−3496.
(13) Liu, S.; Zhao, Q.; Li, Q.; Zhang, H.; You, L.; Zhang, J.; Yu, D. *Nanotechnology* **2011**, *22*, 115302.
(14) Storm, A. J.; Chen, J. H.; Ling, X. S.; Zandbergen, H. W.; Dekker, C. *Nat. Mater.* **2003**, *2*, 537−540.
(15) Ivanov, A. P.; Instuli, E.; McGilvery, C. M.; Baldwin, G.; McComb, D. W.; Albrecht, T.; Edel, J. B. *Nano Lett.* **2011**, *11*, 279−285.
(16) Uddin, A.; Yemenicioglu, S.; Chen, C. H.; Corigliano, E.; Milaninia, K.; Theogarajan, L. *Nanotechnology* **2013**, *24*, 155501.
(17) Kuan, A. T.; Golovchenko, J. A. *Appl. Phys. Lett.* **2012**, *100*, 213104.
(18) Yang, J. J.; Ferranti, D. C.; Stern, L. A.; Sanford, C. A.; Huang, J.; Ren, Z.; Qin, L. C.; Hall, A. R. *Nanotechnology* **2011**, *22*, 285310.

(19) Sawafta, F.; Clancy, B.; Carlsen, A. T.; Huber, M.; Hall, A. R. *Nanoscale* **2014**, *6*, 6991−6996.

(20) Li, J.; Stein, D.; McMullan, C.; Branton, D.; Aziz, M. J.; Golovchenko, J. A. *Nature* **2001**, *412*, 166−169.

(21) Liu, S.; Yuzvinsky, T. D.; Schmidt, H. *ACS Nano* **2013**, *7*, 5621−5627.

(22) Apel, P. Y.; Blonskaya, I. V.; Orelovitch, O. L.; Ramirez, P.; Sartowska, B. A. *Nanotechnology* **2011**, *22*, 175302.

(23) Wu, Z. Y.; Li, C. Y.; Guo, X. L.; Li, B.; Zhang, D. W.; Xu, Y.; Fang, F. *Lab Chip* **2012**, *12*, 3408−3412.

(24) James, T.; Kalinin, Y. V.; Chan, C. C.; Randhawa, J. S.; Gaevski, M.; Gracias, D. H. *Nano Lett.* **2012**, *12*, 3437−3442.

(25) Deng, T.; Li, M.; Chen, J.; Wang, Y.; Liu, Z. *J. Phys. Chem. C* **2014**, *118*, 18110−18115.

(26) Burouni, N.; Berenschot, E.; Elwenspoek, M.; Sarajlic, E.; Leussink, P.; Jansen, H.; Tas, N. *Nanotechnology* **2013**, *24*, 285303.

(27) Wu, S.; Wildhaber, F.; Vazquez-Mena, O.; Bertsch, A.; Brugger, J.; Renaud, P. *Nanoscale* **2012**, *4*, 5718−5723.

(28) Shin, S.; Kim, B. S.; Song, J.; Lee, H.; Cho, H. H. *Lab Chip* **2012**, *12*, 2568−2574.

(29) Pardon, G.; Gatty, H. K.; Stemme, G.; van der Wijngaart, W.; Roxhed, N. *Nanotechnology* **2013**, *24*, 015602.

(30) Xia, D.; Yan, J.; Hou, S. *Small* **2012**, *8*, 2787−2801.

(31) Heo, J.; Kwon, H. J.; Jeon, H.; Kim, B.; Kim, S. J.; Lim, G. *Nanoscale* **2014**, *6*, 9681−9688.

(32) Harms, Z. D.; Mogensen, K. B.; Nunes, P. S.; Zhou, K.; Hildenbrand, B. W.; Mitra, I.; Tan, Z.; Zlotnick, A.; Kutter, J. P.; Jacobson, S. C. *Anal. Chem.* **2011**, *83*, 9573−9578.

(33) Kim, S. H.; Cui, Y.; Lee, M. J.; Nam, S. W.; Oh, D.; Kang, S. H.; Kim, Y. S.; Park, S. *Lab Chip* **2011**, *11*, 348−353.

(34) Perry, J. M.; Harms, Z. D.; Jacobson, S. C. *Small* **2012**, *8*, 1521−1526.

(35) Guan, W.; Rajan, N. K.; Duan, X.; Reed, M. A. *Lab Chip* **2013**, *13*, 1431−1436.

(36) Lesser-Rojas, L.; Sriram, K. K.; Liao, K. T.; Lai, S. C.; Kuo, P. C.; Chu, M. L.; Chou, C. F. *Biomicrofluidics* **2014**, *8*, 016501.

(37) Haywood, D. G.; Harms, Z. D.; Jacobson, S. C. *Anal. Chem.* **2014**, *86*, 11174−11180.

(38) Menard, L. D.; Mair, C. E.; Woodson, M. E.; Alarie, J. P.; Ramsey, J. M. *ACS Nano* **2012**, *6*, 9087−9094.

(39) Menard, L. D.; Ramsey, J. M. *Anal. Chem.* **2013**, *85*, 1146−1153.

(40) Menard, L. D.; Ramsey, J. M. *Nano Lett.* **2011**, *11*, 512−517.

(41) Angeli, E.; Manneschi, C.; Repetto, L.; Firpo, G.; Valbusa, U. *Lab Chip* **2011**, *11*, 2625−2629.

(42) Fanzio, P.; Mussi, V.; Manneschi, C.; Angeli, E.; Firpo, G.; Repetto, L.; Valbusa, U. *Lab Chip* **2011**, *11*, 2961−2966.

(43) Manneschi, C.; Fanzio, P.; Angeli, E.; Firpo, G.; Ceseracciu, L.; Mussi, V.; Repetto, L.; Valbusa, U. *Microfluid. Nanofluid.* **2012**, *14*, 21−30.

(44) Hendricks, N. R.; Watkins, J. J.; Carter, K. R. *J. Mater. Chem.* **2011**, *21*, 14213−14218.

(45) Mikkelsen, M. B.; Letailleur, A. A.; Sondergard, E.; Barthel, E.; Teisseire, J.; Marie, R.; Kristensen, A. *Lab Chip* **2012**, *12*, 262−267.

(46) Chantiwas, R.; Park, S.; Soper, S. A.; Kim, B. C.; Takayama, S.; Sunkara, V.; Hwang, H.; Cho, Y. K. *Chem. Soc. Rev.* **2011**, *40*, 3677−3702.

(47) Yin, Z.; Cheng, E.; Zou, H. *Lab Chip* **2014**, *14*, 1614−1621.

(48) Raidongia, K.; Huang, J. *J. Am. Chem. Soc.* **2012**, *134*, 16528−16531.

(49) Kleinert, J.; Kim, S.; Velev, O. D. *Langmuir* **2012**, *28*, 3037−3044.

(50) Elsamadisi, P.; Wang, Y.; Velmurugan, J.; Mirkin, M. V. *Anal. Chem.* **2011**, *83*, 671−673.

(51) Steinbock, L. J.; Steinbock, J. F.; Radenovic, A. *Nano Lett.* **2013**, *13*, 1717−1723.

(52) Lazenby, R. A.; McKelvey, K.; Peruffo, M.; Baghdadi, M.; Unwin, P. R. *J. Solid State Electrochem.* **2013**, *17*, 2979−2987.

(53) Thakar, R.; Weber, A. E.; Morris, C. A.; Baker, L. A. *Analyst* **2013**, *138*, 5973−5982.

(54) Kim, Y. T.; Scarnulis, D. M.; Ewing, A. G. *Anal. Chem.* **1986**, *58*, 1782−1786.

(55) Takahashi, Y.; Shevchuk, A. I.; Novak, P.; Zhang, Y. J.; Ebejer, N.; Macpherson, J. V.; Unwin, P. R.; Pollard, A. J.; Roy, D.; Clifford, C. A.; Shiku, H.; Matsue, T.; Klenerman, D.; Korchev, Y. E. *Angew. Chem., Int. Ed.* **2011**, *50*, 9638−9642.

(56) Yu, Y.; Noel, J. M.; Mirkin, M. V.; Gao, Y.; Mashtalir, O.; Friedman, G.; Gogotsi, Y. *Anal. Chem.* **2014**, *86*, 3365−3372.

(57) Takahashi, Y.; Shevchuk, A. I.; Novak, P.; Murakami, Y.; Shiku, H.; Korchev, Y. E.; Matsue, T. *J. Am. Chem. Soc.* **2010**, *132*, 10118−10126.

(58) Actis, P.; Tokar, S.; Clausmeyer, J.; Babakinejad, B.; Mikhaleva, S.; Cornut, R.; Takahashi, Y.; Cordoba, A. L.; Novak, P.; Shevchuck, A. I.; Dougan, J. A.; Kazarian, S. G.; Gorelkin, P. V.; Erofeev, A. S.; Yaminsky, I. V.; Unwin, P. R.; Schuhmann, W.; Klenerman, D.; Rusakov, D. A.; Sviderskaya, E. V.; Korchev, Y. E. *ACS Nano* **2014**, *8*, 875−884.

(59) Zhu, X. Y.; Qiao, Y. H.; Zhang, X.; Zhang, S. S.; Yin, X. H.; Gu, J.; Chen, Y.; Zhu, Z. W.; Li, M. X.; Shao, Y. H. *Anal. Chem.* **2014**, *86*, 7001−7008.

(60) Bard, A. J.; Faulkner, L. R. *Electrochemical Methods*; John Wiley and Sons: New York, 1980.

(61) Hatsuki, R.; Yujiro, F.; Yamamoto, T. *Microfluid. Nanofluid.* **2012**, *14*, 983−988.

(62) Kazoe, Y.; Mawatari, K.; Sugii, Y.; Kitamori, T. *Anal. Chem.* **2011**, *83*, 8152−8157.

(63) Vitarelli, M. J.; Prakash, S.; Talaga, D. S. *Anal. Chem.* **2011**, *83*, 533−541.

(64) Hunter, R. J. *Zeta Potential in Colloid Science*; Academic Press, Inc.: San Diego, CA, 1981.

(65) Perry, J. M.; Zhou, K.; Harms, Z. D.; Jacobson, S. C. *ACS Nano* **2010**, *4*, 3897−3902.

(66) Stein, D.; Kruithof, M.; Dekker, C. *Phys. Rev. Lett.* **2004**, *93*, 035901.

(67) Lee, C.; Joly, L.; Siria, A.; Biance, A. L.; Fulcrand, R.; Bocquet, L. *Nano Lett.* **2012**, *12*, 4037−4044.

(68) Tagliazucchi, M.; Rabin, Y.; Szleifer, I. *J. Am. Chem. Soc.* **2011**, *133*, 17753−17763.

(69) Burgreen, D.; Nakache, F. R. *J. Phys. Chem.* **1964**, *68*, 1084.

(70) Levine, S.; Marriott, J. R.; Robinson, K. *J. Chem. Soc. Faraday Trans. 2* **1975**, *71*, 1−11.

(71) Rice, C. L.; Whitehead, R. *J. Phys. Chem.* **1965**, *69*, 4017.

(72) Yeh, L.-H.; Xue, S.; Joo, S. W.; Qian, S.; Hsu, J.-P. *J. Phys. Chem. C* **2012**, *116*, 4209−4216.

(73) Cao, Q.; Zuo, C.; Li, L.; Zhang, Y. *Microfluid. Nanofluid.* **2011**, *12*, 649−655.

(74) Xia, L.; Dutta, D. *Analyst* **2013**, *138*, 2126−2133.

(75) Wang, C. M.; Wang, L.; Zhu, X. R.; Wang, Y. G.; Xue, J. M. *Lab Chip* **2012**, *12*, 1710−1716.

(76) Pennathur, S.; Santiago, J. G. *Anal. Chem.* **2005**, *77*, 6782−6789.

(77) Hsu, J. P.; Yee, C. P.; Yeh, L. H. *Langmuir* **2012**, *28*, 10942−10947.

(78) Huang, C.-H.; Lee, E. *J. Phys. Chem. C* **2012**, *116*, 15058−15067.

(79) Andersen, M. B.; Bruus, H.; Bardhan, J. P.; Pennathur, S. *J. Colloid Interface Sci.* **2011**, *360*, 262−271.

(80) Bandopadhyay, A.; Hossain, S. S.; Chakraborty, S. *Langmuir* **2014**, *30*, 7251−7258.

(81) Chakraborty, J.; Dey, R.; Chakraborty, S. *Phys. Rev. E* **2012**, *86*, 061504.

(82) Dutta, D. *Microfluid. Nanofluid.* **2010**, *10*, 691−696.

(83) Das, S.; Guha, A.; Mitra, S. K. *Anal. Chim. Acta* **2013**, *804*, 159−166.

(84) Cheng, L. J.; Guo, L. J. *Chem. Soc. Rev.* **2010**, *39*, 923−938.

(85) Wei, C.; Bard, A. J.; Feldberg, S. W. *Anal. Chem.* **1997**, *69*, 4627−4633.

(86) Siwy, Z.; Fulinski, A. *Phys. Rev. Lett.* **2002**, *89*, 198103.

(87) Liu, J.; Wang, D.; Kvetny, M.; Brown, W.; Li, Y.; Wang, G. *Langmuir* **2013**, *29*, 8743−8752.

(88) Momotenko, D.; Girault, H. H. *J. Am. Chem. Soc.* **2011**, *133*, 14496−14499.

(89) Yeh, L. H.; Hughes, C.; Zeng, Z.; Qian, S. *Anal. Chem.* **2014**, *86*, 2681−2686.

(90) Yeh, L. H.; Zhang, M.; Qian, S. *Anal. Chem.* **2013**, *85*, 7527−7534.

(91) Liu, J.; Wang, D.; Kvetny, M.; Brown, W.; Li, Y.; Wang, G. *Anal. Chem.* **2012**, *84*, 6926−6929.

(92) Wu, S.; Wildhaber, F.; Bertsch, A.; Brugger, J.; Renaud, P. *Appl. Phys. Lett.* **2013**, *102*, 213108.

(93) Zhang, H.; Hou, X.; Zeng, L.; Yang, F.; Li, L.; Yan, D.; Tian, Y.; Jiang, L. *J. Am. Chem. Soc.* **2013**, *135*, 16102−16110.

(94) Nasir, S.; Ali, M.; Ensinger, W. *Nanotechnology* **2012**, *23*, 225502.

(95) Wang, G. L.; Bohaty, A. K.; Zharov, I.; White, H. S. *J. Am. Chem. Soc.* **2006**, *128*, 13553−13558.

(96) Ali, M.; Nasir, S.; Ramirez, P.; Ahmed, I.; Nguyen, Q. H.; Fruk, L.; Mafe, S.; Ensinger, W. *Adv. Funct. Mater.* **2012**, *22*, 390−396.

(97) Buchsbaum, S. F.; Nguyen, G.; Howorka, S.; Siwy, Z. S. *J. Am. Chem. Soc.* **2014**, *136*, 9902−9905.

(98) Pevarnik, M.; Healy, K.; Davenport, M.; Yen, J.; Siwy, Z. S. *Analyst* **2012**, *137*, 2944−2950.

(99) Wen, L.; Liu, Q.; Ma, J.; Tian, Y.; Li, C.; Bo, Z.; Jiang, L. *Adv. Mater.* **2012**, *24*, 6193−6198.

(100) Zhang, M.; Hou, X.; Wang, J.; Tian, Y.; Fan, X.; Zhai, J.; Jiang, L. *Adv. Mater.* **2012**, *24*, 2424−2428.

(101) Ali, M.; Ramirez, P.; Nguyen, H.; Nasir, S.; Cervera, J.; Mafe, S.; Ensinger, W. *ACS Nano* **2012**, *6*, 3631−3640.

(102) Zhang, L.-X.; Cai, S.-L.; Zheng, Y.-B.; Cao, X.-H.; Li, Y.-Q. *Adv. Funct. Mater.* **2011**, *21*, 2103−2107.

(103) Wen, L. P.; Ma, J.; Tian, Y.; Zhai, J.; Jiang, L. *Small* **2012**, *8*, 838−842.

(104) Li, C.-Y.; Ma, F.-X.; Wu, Z.-Q.; Gao, H.-L.; Shao, W.-T.; Wang, K.; Xia, X.-H. *Adv. Funct. Mater.* **2013**, *23*, 3836−3844.

(105) Meng, Z.; Jiang, C.; Li, X.; Zhai, J. *ACS Appl. Mater. Interfaces* **2014**, *6*, 3794−3798.

(106) Ali, M.; Nasir, S.; Nguyen, Q. H.; Sahoo, J. K.; Tahir, M. N.; Tremel, W.; Ensinger, W. *J. Am. Chem. Soc.* **2011**, *133*, 17307−17314.

(107) Han, C. P.; Hou, X.; Zhang, H. C.; Guo, W.; Li, H. B.; Jiang, L. *J. Am. Chem. Soc.* **2011**, *133*, 7644−7647.

(108) Ali, M.; Ramirez, P.; Nasir, S.; Nguyen, Q.-H.; Ensinger, W.; Mafe, S. *Appl. Phys. Lett.* **2014**, *104*, 043703.

(109) Cao, L.; Guo, W.; Wang, Y.; Jiang, L. *Langmuir* **2012**, *28*, 2194−2199.

(110) Luo, L.; Holden, D. A.; White, H. S. *ACS Nano* **2014**, *8*, 3023−3030.

(111) Luo, L.; Holden, D. A.; Lan, W.-J.; White, H. S. *ACS Nano* **2012**, *6*, 6507−6514.

(112) Lan, W.-J.; Holden, D. A.; White, H. S. *J. Am. Chem. Soc.* **2011**, *133*, 13300−13303.

(113) Gamble, T.; Decker, K.; Plett, T. S.; Pevarnik, M.; Pietschmann, J.-F.; Vlassiouk, I.; Aksimentiev, A.; Siwy, Z. S. *J. Phys. Chem. C* **2014**, *118*, 9809−9819.

(114) Yan, Y.; Wang, L.; Xue, J.; Chang, H. C. *J. Chem. Phys.* **2013**, *138*, 044706.

(115) Yeh, L. H.; Zhang, M.; Hu, N.; Joo, S. W.; Qian, S.; Hsu, J. P. *Nanoscale* **2012**, *4*, 5169−5177.

(116) Xue, S.; Yeh, L.-H.; Ma, Y.; Qian, S. *J. Phys. Chem. C* **2014**, *118*, 6090−6099.

(117) Kubeil, C.; Bund, A. *J. Phys. Chem. C* **2011**, *115*, 7866−7873.

(118) Vilozny, B.; Wollenberg, A. L.; Actis, P.; Hwang, D.; Singaram, B.; Pourmand, N. *Nanoscale* **2013**, *5*, 9214−9221.

(119) He, H.; Xu, X.; Jin, Y. *Anal. Chem.* **2014**, *86*, 4815−4821.

(120) Liu, S.; Dong, Y.; Zhao, W.; Xie, X.; Ji, T.; Yin, X.; Liu, Y.; Liang, Z.; Momotenko, D.; Liang, D.; Girault, H. H.; Shao, Y. *Anal. Chem.* **2012**, *84*, 5565−5573.

(121) Deng, X. L.; Takami, T.; Son, J. W.; Kang, E. J.; Kawai, T.; Park, B. H. *Sci. Rep.* **2014**, *4*, 4005.

(122) Actis, P.; Vilozny, B.; Seger, R. A.; Li, X.; Jejelowo, O.; Rinaudo, M.; Pourmand, N. *Langmuir* **2011**, *27*, 6528−6533.

(123) Umehara, S.; Pourmand, N.; Webb, C. D.; Davis, R. W.; Yasuda, K.; Karhanek, M. *Nano Lett.* **2006**, *6*, 2486−2492.

(124) Sa, N.; Baker, L. A. *J. Electrochem. Soc.* **2013**, *160*, H376−H381.

(125) Clarke, R. W.; Zhukov, A.; Richards, O.; Johnson, N.; Ostanin, V.; Klenerman, D. *J. Am. Chem. Soc.* **2013**, *135*, 322−329.

(126) McKelvey, K.; Kinnear, S. L.; Perry, D.; Momotenko, D.; Unwin, P. R. *J. Am. Chem. Soc.* **2014**, *136*, 13735−13744.

(127) Sa, N.; Baker, L. A. *J. Am. Chem. Soc.* **2011**, *133*, 10398−401.

(128) Sa, N.; Lan, W. J.; Shi, W. Q.; Baker, L. A. *ACS Nano* **2013**, *7*, 11272−11282.

(129) Singh, K. P.; Kumar, M. *J. Appl. Phys.* **2011**, *110*, 084322.

(130) Hu, N.; Ai, Y.; Qian, S. *Sens. Actuators, B: Chem.* **2012**, *161*, 1150−1167.

(131) Matovic, J.; Adamovic, N.; Radovanovic, F.; Jakšić, Z.; Schmid, U. *Sens. Actuators, B: Chem.* **2012**, *170*, 137−142.

(132) Cheng, L. S.; Cao, D. P. *ACS Nano* **2011**, *5*, 1102−1108.

(133) Gabrielsson, E. O.; Berggren, M. *Biomicrofluidics* **2013**, *7*, 64117.

(134) Gabrielsson, E. O.; Tybrandt, K.; Berggren, M. *Lab Chip* **2012**, *12*, 2507−2513.

(135) Grattoni, A.; Fine, D.; Zabre, E.; Ziemys, A.; Gill, J.; Mackeyev, Y.; Cheney, M. A.; Danila, D. C.; Hosali, S.; Wilson, L. J.; Hussain, F.; Ferrari, M. *ACS Nano* **2011**, *5*, 9382−9391.

(136) Guan, W.; Fan, R.; Reed, M. A. *Nat. Commun.* **2011**, *2*, 506.

(137) Paik, K. H.; Liu, Y.; Tabard-Cossa, V.; Waugh, M. J.; Huber, D. E.; Provine, J.; Howe, R. T.; Dutton, R. W.; Davis, R. W. *ACS Nano* **2012**, *6*, 6767−6775.

(138) Jin, X. Z.; Aluru, N. R. *Microfluid. Nanofluid.* **2011**, *11*, 297−306.

(139) Singh, K. P.; Kumari, K.; Kumar, M. *J. Appl. Phys.* **2011**, *110*, 084301.

(140) Jiang, Z.; Stein, D. *Phys. Rev. E* **2011**, *83*, 031203.

(141) Rutkowska, A.; Edel, J. B.; Albrecht, T. *ACS Nano* **2013**, *7*, 547−555.

(142) Zeng, L.; Yang, Z.; Zhang, H.; Hou, X.; Tian, Y.; Yang, F.; Zhou, J.; Li, L.; Jiang, L. *Small* **2014**, *10*, 793−801.

(143) Kong, Y.; Fan, X.; Zhang, M.; Hou, X.; Liu, Z.; Zhai, J.; Jiang, L. *ACS Appl. Mater. Interfaces* **2013**, *5*, 7931−7936.

(144) Segerink, L. I.; Eijkel, J. C. T. *Lab Chip* **2014**, *14*, 3201−3205.

(145) Zhou, K.; Kovarik, M. L.; Jacobson, S. C. *J. Am. Chem. Soc.* **2008**, *130*, 8614.

(146) Quist, J.; Trietsch, S. J.; Vulto, P.; Hankemeier, T. *Lab Chip* **2013**, *13*, 4810−4815.

(147) Gong, M. M.; Zhang, P.; MacDonald, B. D.; Sinton, D. *Anal. Chem.* **2014**, *86*, 8090−8097.

(148) Jen, C. P.; Amstislavskaya, T. G.; Kuo, C. C.; Chen, Y. H. *PLoS One* **2014**, *9*, e102050.

(149) Wang, J.; Xu, Z.; Li, Y.; Liu, C.; Liu, J.; Chen, L.; Du, L.; Wang, L. *Appl. Phys. Lett.* **2013**, *103*, 043103.

(150) Cho, I.; Sung, G. Y.; Kim, S. J. *Nanoscale* **2014**, *6*, 4620−4626.

(151) Wang, C.; Ouyang, J.; Wang, Y. Y.; Ye, D. K.; Xia, X. H. *Anal. Chem.* **2014**, *86*, 3216−3221.

(152) Zhang, D.-W.; Zhang, H.-Q.; Tian, L.; Wang, L.; Fang, F.; Liu, K.; Wu, Z.-Y. *Microfluid. Nanofluid.* **2012**, *14*, 69−76.

(153) Louer, A. C.; Plecis, A.; Pallandre, A.; Galas, J. C.; Estevez-Torres, A.; Haghiri-Gosnet, A. M. *Anal. Chem.* **2013**, *85*, 7948−7956.

(154) Liao, K. T.; Chou, C. F. *J. Am. Chem. Soc.* **2012**, *134*, 8742−8745.

(155) Aizel, K.; Agache, V.; Pudda, C.; Bottausci, F.; Fraisseix, C.; Bruniaux, J.; Navarro, F.; Fouillet, Y. *Lab Chip* **2013**, *13*, 4476−4485.

(156) Startsev, M. A.; Inglis, D. W.; Baker, M. S.; Goldys, E. M. *Anal. Chem.* **2013**, *85*, 7133−7138.

(157) Hsu, W. L.; Harvie, D. J.; Davidson, M. R.; Jeong, H.; Goldys, E. M.; Inglis, D. W. *Lab Chip* **2014**, *14*, 3539−3549.

(158) Inglis, D. W.; Goldys, E. M.; Calander, N. P. *Angew. Chem., Int. Ed.* **2011**, *50*, 7546−7550.

(159) Chang, C. C.; Yeh, C. P.; Yang, R. J. *Electrophoresis* **2012**, *33*, 758−764.

(160) Mai, J.; Miller, H.; Hatch, A. *ACS Nano* **2012**, *6*, 10206−10215.

(161) Hlushkou, D.; Perry, J. M.; Jacobson, S. C.; Tallarek, U. *Anal. Chem.* **2012**, *84*, 267−274.

(162) Jia, M.; Kim, T. *Anal. Chem.* **2014**, *86*, 7360−7367.

(163) Di Ventra, M. *Methods Mol. Biol.* **2012**, *870*, 149−163.

(164) Di Ventra, M. *Nanotechnology* **2013**, *24*, 342501.

(165) Li, Y.; Zheng, Y.; Zare, R. N. *ACS Nano* **2012**, *6*, 993−997.

(166) Steinbock, L. J.; Bulushev, R. D.; Krishnan, S.; Raillon, C.; Radenovic, A. *ACS Nano* **2013**, *7*, 11255−11262.

(167) Vogel, R.; Willmott, G.; Kozak, D.; Roberts, G. S.; Anderson, W.; Groenewegen, L.; Glossop, B.; Barnett, A.; Turner, A.; Trau, M. *Anal. Chem.* **2011**, *83*, 3499−3506.

(168) Wanunu, M.; Bhattacharya, S.; Xie, Y.; Tor, Y.; Aksimentiev, A.; Drndic, M. *ACS Nano* **2011**, *5*, 9345−9353.

(169) Freedman, K. J.; Bastian, A. R.; Chaiken, I.; Kim, M. J. *Small* **2013**, *9*, 750−759.

(170) Liu, Q.; Wu, H.; Wu, L.; Xie, X.; Kong, J.; Ye, X.; Liu, L. *PLoS One* **2012**, *7*, e46014.

(171) Pevarnik, M.; Healy, K.; Toimil-Molares, M. E.; Morrison, A.; Letant, S. E.; Siwy, Z. S. *ACS Nano* **2012**, *6*, 7295−7302.

(172) Pevarnik, M.; Schiel, M.; Yoshimatsu, K.; Vlassiouk, I. V.; Kwon, J. S.; Shea, K. J.; Siwy, Z. S. *ACS Nano* **2013**, *7*, 3720−3728.

(173) Arjmandi, N.; Van Roy, W.; Lagae, L.; Borghs, G. *Anal. Chem.* **2012**, *84*, 8490−8496.

(174) Booth, M. A.; Vogel, R.; Curran, J. M.; Harbison, S.; Travas-Sejdic, J. *Biosens. Bioelectron.* **2013**, *45*, 136−140.

(175) Eldridge, J. A.; Willmott, G. R.; Anderson, W.; Vogel, R. *J. Colloid Interface Sci.* **2014**, *429*, 45−52.

(176) Kozak, D.; Anderson, W.; Vogel, R.; Chen, S.; Antaw, F.; Trau, M. *ACS Nano* **2012**, *6*, 6990−6997.

(177) German, S. R.; Luo, L.; White, H. S.; Mega, T. L. *J. Phys. Chem. C* **2013**, *117*, 703−711.

(178) Vogel, R.; Anderson, W.; Eldridge, J.; Glossop, B.; Willmott, G. *Anal. Chem.* **2012**, *84*, 3125−3131.

(179) Kawano, R.; Osaki, T.; Sasaki, H.; Takinoue, M.; Yoshizawa, S.; Takeuchi, S. *J. Am. Chem. Soc.* **2011**, *133*, 8474−8477.

(180) Gupta, C.; Liao, W. C.; Gallego-Perez, D.; Castro, C. E.; Lee, L. J. *Biomicrofluidics* **2014**, *8*, 024114.

(181) Billinge, E. R.; Broom, M.; Platt, M. *Anal. Chem.* **2014**, *86*, 1030−1037.

(182) Fanzio, P.; Manneschi, C.; Angeli, E.; Mussi, V.; Firpo, G.; Ceseracciu, L.; Repetto, L.; Valbusa, U. *Sci. Rep.* **2012**, *2*, 791.

(183) Colby, A. H.; Colson, Y. L.; Grinstaff, M. W. *Nanoscale* **2013**, *5*, 3496−3504.

(184) Willmott, G. R.; Parry, B. E. T. *J. Appl. Phys.* **2011**, *109*, 094307.

(185) Tsutsui, M.; Hongo, S.; He, Y. H.; Taniguchi, M.; Gemma, N.; Kawai, T. *ACS Nano* **2012**, *6*, 3499−3505.

(186) Pedone, D.; Langecker, M.; Abstreiter, G.; Rant, U. *Nano Lett.* **2011**, *11*, 1561−1567.

(187) Kurz, V.; Nelson, E. M.; Shim, J.; Timp, G. *ACS Nano* **2013**, *7*, 4057−4069.

(188) Albrecht, T. *Nat. Nanotechnol.* **2011**, *6*, 195−196.

(189) Yusko, E. C.; Johnson, J. M.; Majd, S.; Prangkio, P.; Rollings, R. C.; Li, J.; Yang, J.; Mayer, M. *Nat. Nanotechnol.* **2011**, *6*, 253−260.

(190) Zhou, K.; Li, L.; Tan, Z.; Zlotnick, A.; Jacobson, S. C. *J. Am. Chem. Soc.* **2011**, *133*, 1618−21.

(191) Anderson, B. N.; Muthukumar, M.; Meller, A. *ACS Nano* **2013**, *7*, 1408−1414.

(192) Tsutsui, M.; Rahong, S.; Iizumi, Y.; Okazaki, T.; Taniguchi, M.; Kawai, T. *Sci. Rep.* **2011**, *1*, 46.

(193) Balakrishnan, K. R.; Anwar, G.; Chapman, M. R.; Nguyen, T.; Kesavaraju, A.; Sohn, L. L. *Lab Chip* **2013**, *13*, 1302−1307.

(194) Yukimoto, N.; Tsutsui, M.; He, Y.; Shintaku, H.; Tanaka, S.; Kawano, S.; Kawai, T.; Taniguchi, M. *Sci. Rep.* **2013**, *3*, 1855.

(195) Wilson, J.; Di Ventra, M. *Nanotechnology* **2013**, *24*, 415101.

(196) Traversi, F.; Raillon, C.; Benameur, S. M.; Liu, K.; Khlybov, S.; Tosun, M.; Krasnozhon, D.; Kis, A.; Radenovic, A. *Nat. Nanotechnol.* **2013**, *8*, 939−945.

(197) Prasongkit, J.; Grigoriev, A.; Pathak, B.; Ahuja, R.; Scheicher, R. H. *J. Phys. Chem. C* **2013**, *117*, 15421−15428.

(198) Xie, P.; Xiong, Q.; Fang, Y.; Qing, Q.; Lieber, C. M. *Nat. Nanotechnol.* **2012**, *7*, 119−125.

(199) Langecker, M.; Pedone, D.; Simmel, F. C.; Rant, U. *Nano Lett.* **2011**, *11*, 5002−5007.

(200) Saha, K. K.; Drndic, M.; Nikolic, B. K. *Nano Lett.* **2012**, *12*, 50−55.

(201) Lan, W.-J.; Holden, D. A.; Zhang, B.; White, H. S. *Anal. Chem.* **2011**, *83*, 3840−3847.

(202) Lan, W.-J.; Kubeil, C.; Xiong, J.-W.; Bund, A.; White, H. S. *J. Phys. Chem. C* **2014**, *118*, 2726−2734.

(203) Roberts, G. S.; Yu, S.; Zeng, Q. L.; Chan, L. C. L.; Anderson, W.; Colby, A. H.; Grinstaff, M. W.; Reid, S.; Vogel, R. *Biosens. Bioelectron.* **2012**, *31*, 17−25.

(204) Terejanszky, P.; Makra, I.; Furjes, P.; Gyurcsanyi, R. E. *Anal. Chem.* **2014**, *86*, 4688−4697.

(205) Wang, Y.; Kececi, K.; Mirkin, M. V.; Mani, V.; Sardesai, N.; Rusling, J. F. *Chem. Sci.* **2013**, *4*, 655−663.

(206) Steinbock, L. J.; Lucas, A.; Otto, O.; Keyser, U. F. *Electrophoresis* **2012**, *33*, 3480−3487.

(207) Gong, X. Q.; Patil, A. V.; Ivanov, A. P.; Kong, Q. Y.; Gibb, T.; Dogan, F.; deMello, A. J.; Edel, J. B. *Anal. Chem.* **2014**, *86*, 835−841.

(208) Li, W.; Bell, N. A. W.; Hernandez-Ainsa, S.; Thacker, V. V.; Thackray, A. M.; Bujdoso, R.; Keyser, U. F. *ACS Nano* **2013**, *7*, 4129−4134.

(209) Kumar, S.; Xuan, J.; Lee, M. L.; Tolley, H. D.; Hawkins, A. R.; Woolley, A. T. *Lab Chip* **2013**, *13*, 4591−4598.

(210) De Bruyne, S.; De Malsche, W.; Fekete, V.; Thienpont, H.; Ottevaere, H.; Gardeniers, H.; Desmet, G. *Analyst* **2013**, *138*, 6127−6133.

(211) Le, T. H.; Mawatari, K.; Shimizu, H.; Kitamori, T. *Analyst* **2014**, *139*, 2721−2725.

(212) Shimizu, H.; Mawatari, K.; Kitamori, T. *Analyst* **2014**, *139*, 2154−2157.

(213) O'Hern, S. C.; Stewart, C. A.; Boutilier, M. S. H.; Idrobo, J. C.; Bhaviripudi, S.; Das, S. K.; Kong, J.; Laoui, T.; Atieh, M.; Karnik, R. *ACS Nano* **2012**, *6*, 10130−10138.

(214) Nadtochiy, A.; Melnikov, D.; Gracheva, M. *ACS Nano* **2013**, *7*, 7053−7061.

(215) Gillespie, D.; Pennathur, S. *Anal. Chem.* **2013**, *85*, 2991−2998.

(216) Jubery, T. Z.; Prabhu, A. S.; Kim, M. J.; Dutta, P. *Electrophoresis* **2012**, *33*, 325−333.

(217) Regtmeier, J.; Kasewieter, J.; Everwand, M.; Anselmetti, D. *J. Sep. Sci.* **2011**, *34*, 1180−1183.

(218) Viefhues, M.; Regtmeier, J.; Anselmetti, D. *Analyst* **2013**, *138*, 186−196.

(219) Cao, Z.; Yobas, L. *Anal. Chem.* **2014**, *86*, 737−743.

(220) Russell, A. J.; Del Bonis-O'Donnell, J. T.; Wynne, T. M.; Napoli, M. T.; Pennathur, S. *Electrophoresis* **2014**, *35*, 412−418.

(221) Choi, S.; Kim, J. M.; Ahn, K. H.; Lee, S. J. *Electrophoresis* **2014**, *35*, 2068−2077.

(222) Kovarik, M. L.; Jacobson, S. C. *Anal. Chem.* **2007**, *79*, 1655−1660.

(223) Mathwig, K.; Lemay, S. G. *Micromachines* **2013**, *4*, 138−148.

(224) Mawatari, K.; Kubota, S.; Xu, Y.; Priest, C.; Sedev, R.; Ralston, J.; Kitamori, T. *Anal. Chem.* **2012**, *84*, 10812−10816.

(225) Seger, R. A.; Actis, P.; Penfold, C.; Maalouf, M.; Vilozny, B.; Pourmand, N. *Nanoscale* **2012**, *4*, 5843−5846.

(226) Shi, W.; Sa, N.; Thakar, R.; Baker, L. A. *Analyst* **2014**, DOI: 10.1039/C4AN01073F.

(227) Babakinejad, B.; Jonsson, P.; Cordoba, A. L.; Actis, P.; Novak, P.; Takahashi, Y.; Shevchuk, A.; Anand, U.; Anand, P.; Drews, A.; Ferrer-Montiel, A.; Klenerman, D.; Korchev, Y. E. *Anal. Chem.* **2013**, *85*, 9333−9342.

(228) Laforge, F. O.; Carpino, J.; Rotenberg, S. A.; Mirkin, M. V. *Proc. Natl. Acad. Sci. U.S.A* **2007**, *104*, 11895−11900.

(229) Actis, P.; Maalouf, M. M.; Kim, H. J.; Lohith, A.; Vilozny, B.; Seger, R. A.; Pourmand, N. *ACS Nano* **2014**, *8*, 546−553.

(230) Bruckbauer, A.; Zhou, D. J.; Ying, L. M.; Korchev, Y. E.; Abell, C.; Klenerman, D. *J. Am. Chem. Soc.* **2003**, *125*, 9834−9839.

(231) O'Connell, M. A.; Snowden, M. E.; McKelvey, K.; Gayet, F.; Shirley, I.; Haddleton, D. M.; Unwin, P. R. *Langmuir* **2014**, *30*, 10011−10018.

(232) Oja, S. M.; Wood, M.; Zhang, B. *Anal. Chem.* **2013**, *85*, 473−486.

(233) Contento, N. M.; Branagan, S. P.; Bohn, P. W. *Lab Chip* **2011**, *11*, 3634−3641.

(234) Branagan, S. P.; Contento, N. M.; Bohn, P. W. *J. Am. Chem. Soc.* **2012**, *134*, 8617−8624.

(235) Gibson, L. R.; Branagan, S. P.; Bohn, P. W. *Small* **2013**, *9*, 90−97.

(236) Gao, H. L.; Li, C. Y.; Ma, F. X.; Wang, K.; Xu, J. J.; Chen, H. Y.; Xia, X. H. *Phys. Chem. Chem. Phys.* **2012**, *14*, 9460−9467.

(237) Lemay, S. G.; Kang, S.; Mathwig, K.; Singh, P. S. *Acc. Chem. Res.* **2013**, *46*, 369−377.

(238) Zevenbergen, M. A. G.; Singh, P. S.; Goluch, E. D.; Wolfrum, B. L.; Lemay, S. G. *Nano Lett.* **2011**, *11*, 2881−2886.

(239) Huske, M.; Stockmann, R.; Offenhausser, A.; Wolfrum, B. *Nanoscale* **2014**, *6*, 589−598.

(240) Kang, S.; Nieuwenhuis, A.; Mathwig, K.; Mampallil, D.; Lemay, S. G. *ACS Nano* **2013**, *7*, 10931−10937.

(241) Ma, C. X.; Contento, N. M.; Gibson, L. R.; Bohn, P. W. *ACS Nano* **2013**, *7*, 5483−5490.

(242) Fan, F. R.; Bard, A. J. *Science* **1995**, *267*, 871−874.

(243) Sun, P.; Mirkin, M. V. *J. Am. Chem. Soc.* **2008**, *130*, 8241−8250.

(244) Rassaei, L.; Mathwig, K.; Goluch, E. D.; Lemay, S. G. *J. Phys. Chem. C* **2012**, *116*, 10913−10916.

(245) Katelhon, E.; Krause, K. J.; Mathwig, K.; Lemay, S. G.; Wolfrum, B. *ACS Nano* **2014**, *8*, 4924−4930.

(246) Katelhon, E.; Krause, K. J.; Singh, P. S.; Lemay, S. G.; Wolfrum, B. *J. Am. Chem. Soc.* **2013**, *135*, 8874−8881.

(247) Kleijn, S. E. F.; Lai, S. C. S.; Miller, T. S.; Yanson, A. I.; Koper, M. T. M.; Unwin, P. R. *J. Am. Chem. Soc.* **2012**, *134*, 18558−18561.

(248) Yuill, E. M.; Sa, N.; Ray, S. J.; Hieftje, G. M.; Baker, L. A. *Anal. Chem.* **2013**, *85*, 8498−8502.

(249) Metzker, M. L. *Nat. Rev. Genet.* **2010**, *11*, 31−46.

(250) Shendure, J.; Ji, H. L. *Nat. Biotechnol.* **2008**, *26*, 1135−1145.